Evaluation of heterogeneous processes in the polar lower stratosphere in the Whole Atmosphere Community Climate Model

Simone Tilmes,[1] Douglas E. Kinnison,[1] Rolando R. Garcia,[1] Rolf Müller,[2] Fabrizio Sassi,[1] Daniel R. Marsh,[1] and Byron A. Boville[1]

Received 11 December 2006; revised 25 July 2007; accepted 5 September 2007; published 21 December 2007.

[1] Chemical ozone loss in the polar lower stratosphere is derived from an ensemble of three simulations from the Whole Atmosphere Community Climate Model (WACCM3) for the period 1960–2003, using the tracer-tracer correlation technique. We describe a detailed model evaluation of the polar region by applying diagnostics such as vortex temperature, sharpness of the vortex edge, and the potential of activated chlorine (PACl). Meteorological and chemical information about the polar vortex, temperature, vortex size, and activation time, and level of equivalent effective stratospheric chlorine, are included in PACl. Discrepancies of the relationship between chemical ozone loss and PACl between model and observations are discussed. Simulated PACl for Antarctica is in good agreement with observations, owing to slightly lower simulated temperatures and a larger vortex volume than observed. Observed chemical ozone loss of 140 ± 30 DU in the Antarctic vortex core are reproduced by the WACCM3 simulations. However, WACCM3 with the horizontal resolution used here (4 × 5) is not able to simulate the observed sharp transport barrier at the polar vortex edge. Therefore the model does not produce an homogeneous cold polar vortex. Warmer temperatures in the outer region of the vortex result in less chemical ozone loss over the entire polar vortex than observed. For the Arctic, WACCM3 temperatures are biased high (by 2–3 degrees in the annual average) and the vortex volume and chlorine activation period is significantly smaller than observed. WACCM3 Arctic chemical ozone loss only reaches 20 DU for cold winters, where observations suggest ≈80–120 DU.

Citation: Tilmes, S., D. E. Kinnison, R. R. Garcia, R. Müller, F. Sassi, D. R. Marsh, and B. A. Boville (2007), Evaluation of heterogeneous processes in the polar lower stratosphere in the Whole Atmosphere Community Climate Model, *J. Geophys. Res.*, *112*, D24301, doi:10.1029/2006JD008334.

1. Introduction

[2] The composition of the atmosphere has been influenced by human activities, especially during the last several decades. A major focus for stratospheric research has been the study of the ozone hole that was discovered over Antarctica in 1985 [*Farman et al.*, 1985]. Significantly enhanced polar chemical ozone loss is the result of anthropogenic emissions of long-lived halogen compounds (in particular chlorofluorocarbons (CFCs) and halons) into the atmosphere [e.g., *World Meteorological Organization* (*WMO*), 2007]. Observations since 1991 show cumulative annual Antarctic chemical ozone destruction between 120 and 170 Dobson Units (DU) in October in the potential temperature range 350–550 K [*Tilmes et al.*, 2006a]. The amount of Arctic chemical ozone loss is variable, depending on the year-to-year change of meteorological conditions. Climatologically warm winters show almost no chemical ozone destruction, whereas for the cold winter of 2004–2005, maximum accumulated ozone loss reaching Antarctic values have been reported (between 108 DU to 118 DU [e.g., *Jin et al.*, 2006; *von Hobe et al.*, 2006]). It has been shown for the Arctic that chemical ozone loss is controlled by temperature and dynamics of the polar vortex, which can be affected by changing climate conditions [*Rex et al.*, 2004; *Tilmes et al.*, 2006a].

[3] The slowly decreasing stratospheric burden of ozone destroying substances is expected to produce less chemical ozone loss and a reduction of the depth and size of the ozone hole over the coming decades [e.g., *WMO*, 2007; *Newman et al.*, 2006]. Currently, it is not known when the recovery to pre-1980 ozone abundances will be reached as a result of changing atmospheric conditions [*Intergovernmental Panel on Climate Change/Technology and Economic Assessment Panel*, 2005; *Shindell and Grewe*, 2002]. It is expected that changing the ozone distribution will have a

[1] National Center of Atmospheric Research, Boulder, Colorado, USA.
[2] Institute for Stratospheric Chemistry (ICG-1), Forschungszentrum Jülich, Jülich, Germany.

0148-0227/07/2006JD008334

Table 1. Abbreviations Used Frequently in the Text

Abbreviation	Definition
EESC	Equivalent Effective Stratospheric Chlorine
$EESC_n$	normalized EESC
NAT	Nitrate Acid Trihydrate
PSC	Polar Stratospheric Cloud
SAD	Surface Area Densities of sulfate liquid-phase aerosols
STS	Supercooled Ternary Solutions
T_{ACl}	threshold temperature for chlorine activation
T_{PSC}	threshold temperature defined by the NAT equilibrium temperature
PACl	Potential for Activation of Chlorine
$PACl_{met}$	the meteorological part of PACl
PFP	PSC Formation Potential
PV	Potential Vorticity
V_{ACl}	volume of potential chlorine activation
V_{PSC}	volume of potential PSC formation
V_{Vortex}	volume of the vortex
WACCM3	Whole Atmosphere Community Climate Model Version 3

large impact on radiation and temperature and therefore on transport processes in the stratosphere [*Manzini et al.*, 2003; *Langematz et al.*, 2003]. In addition, possible impacts of the Antarctic ozone hole on climate at the Earth's surface have been suggested [*Gillett and Thompson*, 2002; *Sassi et al.*, 2005; *Thompson et al.*, 2005].

[4] To better understand how dynamical and chemical processes may be affected by climate change in the future, comprehensive chemistry-climate models (CCMs) are required. The precise simulation of ozone loss in polar regions is very important for analyzing future climate change. Considering the evolution of the total column ozone in polar regions, significant discrepancies among CCMs, and among model results and observations were found [*Austin et al.*, 2003; *WMO*, 2007; *Eyring et al.*, 2006]. Large discrepancies among models exist, as for Arctic conditions. However, the comparison of the total column ozone between models and observations does not allow a clear distinction between dynamical and chemical processes in the model. Therefore evaluation of chemical ozone loss is desirable. A quantification of chemical loss in column ozone in CCMs is not straightforward and has not been routinely performed. *Lemmen et al.* [2006b] suggested using the tracer-tracer correlation technique [e.g., *Proffitt et al.*, 1993; *Tilmes et al.*, 2004] in CCMs. They applied this technique successfully to results of the ECHAM4.DLR(L39)/CHEM coupled chemistry climate model system [*Hein et al.*, 2001]. Possible shortcomings in applying the technique were discussed. Here, tracer-tracer correlations are employed to derive chemical ozone loss from WACCM3 results (see section 4.2).

[5] To calculate the sensitivity of ozone loss to changes in meteorological conditions, use of the relationship between chemical ozone loss and the potential volume of polar stratospheric cloud (PSC) formation, V_{PSC}, was recommended by the CCM Validation project of Stratospheric Processes and their Role in Climate (SPARC) (CCMVal) [*Eyring et al.*, 2005]. On the basis of observations, this relationship was found to be almost linear [*Rex et al.*, 2004; *Tilmes et al.*, 2004]. Here, we will introduce a measure similar to V_{PSC}, the potential for activation of chlorine (PACl). Besides meteorological information, this diagnostic includes information on the varying equivalent effective stratospheric chlorine (EESC) [*WMO*, 2007; *Newman et al.*, 2006]. The relationship between chemical ozone loss and PACl will be compared between model results and observations. The reasons for the lack of a precise reproduction of this relationship by the model will be analyzed and discussed.

[6] We evaluate the performance of the WACCM3 simulations that represent the historical period between 1950 and 2003. Chemical ozone destruction in the high-latitude lower stratosphere was observed between June and October in the Antarctic and between November and April in the Arctic. In this paper, we will concentrate mainly on these periods, to detect discrepancies between the heterogeneous chemistry in the model and measurements. The unrealistic late break up of the Antarctic polar vortex in WACCM3 was discussed by *Eyring et al.* [2006] and *Garcia et al.* [2007]. Additionally, *Kinnison et al.* [2007] discussed the delayed ozone recovery in a different WACCM version, as a result of the lack of an abrupt final warming. Here, we will not investigate Antarctic processes after October.

[7] A brief description of the model and its ability to estimate heterogeneous processes is given in section 2. Meteorological analyses and observations used in this study are described in section 3. The diagnostics employed to investigate the chemical and meteorological performance of the model during the ozone loss season in polar regions are described in detail in section 4. In section 5, meteorological diagnostics are applied to WACCM3 results. The comparison between PACl and the amount of activated halogen compounds in the model describe the connection between meteorological conditions and chemical processes, namely chemical ozone loss. In section 6, heterogeneous processes and chemical ozone loss derived using tracer-tracer correlations are compared between results derived from WACCM3 and observations for the Arctic and Antarctic regions. The evolution of Antarctic chemical ozone loss is compared in detail with observations for one Antarctic winter. Finally, the relationship between chemical ozone loss and PACl will summarize the results based on the preceding evaluation in section 7. Frequently used abbreviations in this paper are listed in Table 1.

2. WACCM3 Model

[8] WACCM3 is a comprehensive chemistry-climate model with 66 vertical levels from the ground to 4.5×10^{-6} hPa ($\approx$150 km geometric altitude). The vertical resolution of WACCM3 model in the lower stratosphere below 30 km is 1.1–1.4 km. The horizontal resolution used in this study is 4° latitude × 5° longitude. Here, we use instantaneous model output taken every 5 d for meteorological variables and tracers and every 10 d for the surface area densities of sulfate liquid-phase aerosols (SAD). Instantaneous model results have to be considered to derive the location of the polar vortex edge exactly from meteorological variables. A detailed description of the model parameterization and initial and boundary conditions is given by *Garcia et al.* [2007].

[9] WACCM3 has been used to calculate an ensemble of three realizations of the period 1950–2003 denoted as the

reference simulation REF1. The simulations were carried out as part of the CCM validation (CCMVal) activity of the SPARC program [*Eyring et al.*, 2005, 2006] and were used for model intercomparisons [*Eyring et al.*, 2006]. All three realizations, designated as REF1.1, REF1.2, and REF1.3, have been used here. The only difference among these three realizations is a slight perturbation of the initial conditions. Model simulations were done with observed halogens, greenhouse gases, and sea surface temperatures. For this study, the model output is interpolated to specific potential temperature levels ranging from 350 to 600 K, in 25 K steps.

[10] The chemical module of WACCM3 is based upon the three-dimensional (3-D) chemical transport Model of Ozone and Related Chemical Tracers, Version 3 (MOZART-3), described by *Kinnison et al.* [2007]. Chemical rate constants are taken from the JPL02-25 recommendation [*Sander et al.*, 2003]. The heterogeneous reactions in the model, seven reactions on liquid sulfate aerosols, five reaction on solid NAT aerosols, and six reactions on solid water-ice aerosols, are listed by *Kinnison et al.* [2007]. The dimer reaction rate constants are adopted from *Burkholder et al.* [1990] (extended to longer wavelengths) based on *Stimpfle* [2004]. In the WACCM3 simulations, the activation of halogen compounds in polar regions depends on the surface area densities of supercooled ternary solutions (STS) and temperatures. The Aerosol Physical Chemistry Model (ACPM) [*Tabazadeh et al.*, 1994] is used to derive the STS composition. The STS aerosol median radius and SAD is derived following the approach of *Considine et al.* [2000] and is used for the calculation of the rate constant for the heterogeneous reactions, as described by *Kinnison et al.* [2007]. The approach is based on the work by *Drdla et al.* [2002], who showed that approximately 90% of the aerosols observed during the NASA SOLVE/THESEO campaign in the Arctic winter 1999/2000 were of liquid composition. The main part of the chlorine activation in the model occurs therefore on liquid sulfate aerosols [*Kinnison et al.*, 2007].

[11] SAD used in WACCM3 is derived using the SAGE-II and SAMS satellite observations [*Thomason et al.*, 1997] that were updated by *Considine et al.* [2000] and *WMO* [2003]. Unfortunately, in this data set, SAD values in high-latitude regions were set to background values to allow models to derive NAT particles themselves. However, the activation approaches in WACCM3 are mainly based on the occurrence of STS, so that the activation on NAT and water-ice surfaces plays a minor role in this model. Therefore strongly enhanced SAD values occurring after a volcanic eruption are not included in this data set used in WACCM3 and cannot impact chlorine activation in this model version. Thus the impact of volcanic eruptions on chemical ozone loss cannot be addressed here.

3. Meteorological Analysis and Observations

[12] To validate WACCM3 results with a focus on polar regions, UK Meteorological office (MetO) analyses [*Swinbank and O'Neill*, 1994] are used to compare meteorological diagnostics between 1991 and 2006. In addition, we use ECMWF reanalysis data (ERA40) [*Uppala et al.*, 2005] to compare the years between 1958 and 1999, in the way described by *Tilmes et al.* [2006a]. For Antarctica, the years before the satellite era in 1979 will not be investigated because of unreliable data [*Randel et al.*, 2004b; *Simmons et al.*, 2004]. After 1979, ERA40 Antarctic temperatures show a cold bias and an unrealistic vertical structure [*Randel et al.*, 2004a; *Manney et al.*, 2005]. As described by *Tilmes et al.* [2006a], V_{PSC} values based on MetO data are therefore slightly lower than the values derived from ERA40 data.

[13] Chemical ozone loss in the Arctic and Antarctica was derived from observations taken from the Halogen Occultation Experiment (HALOE) aboard the UARS satellite [*Russell et al.*, 1993], and from the Improved Limb Atmospheric Spectrometer (ILAS-II) aboard the ADEOS-II satellite [*Nakajima et al.*, 2006], for the years between 1991 and 2005 and for both hemispheres. HALOE has taken measurements between 1991 and 2005. Because of the occultation geometry, HALOE observations are available for a few days every 2 or 3 months in high polar latitudes. ILAS-II measured during the period between March and October 2003 and between 54°N and 71°N and 64°S to 88°S, thus during an entire Antarctic winter period. A detailed description of the evolution of Antarctic chemical ozone loss was given by *Tilmes et al.* [2006c]. Arctic chemical ozone loss was derived in previous studies [*Tilmes et al.*, 2004, 2007] for winters between 1991 and 1992 and 2002 and 2003 between 380 and 550 K and for the winter 2005 by *von Hobe et al.* [2006] using tracer-tracer correlations. Here, we compare these results to chemical ozone loss derived from WACCM3 results based on the tracer-tracer correlation technique (see section 4.2).

4. Diagnostics for Analyzing Processes Within the Polar Vortex

4.1. Meteorological Diagnostics

[14] Meteorological diagnostics have been derived in the past from observations that show correlations with cumulative chemical ozone loss. A linear relationship between chemical ozone loss and V_{PSC} [*Rex et al.*, 2004; *Tilmes et al.*, 2004] and between chemical ozone loss and the PSC formation potential (PFP) [*Tilmes et al.*, 2006c], has been established. V_{PSC} is the volume where the temperature in the polar vortex is below a threshold temperature defined by the NAT equilibrium temperature, T_{PSC}, based on the formula of *Hanson and Mauersberger* [1988]. Below this temperature, chlorine activation is assumed to occur on NAT surfaces due to the possible existence of PSCs. According to this definition, T_{PSC} depends on pressure and on the concentrations of H_2O and HNO_3. PFP represents the fraction of the vortex, exposed to temperatures below T_{PSC} during the ozone loss season and is defined as $(V_{PSC}/V_{Vortex}) \times$ (activation time/period considered) [*Tilmes et al.*, 2006a]. This measure extends the concept of V_{PSC} to Antarctic conditions. V_{Vortex} is the volume of the entire polar vortex (as defined below). The period for which chlorine activation in the vortex can be expected is referred as "activation time."

[15] *Drdla et al.* [2002] showed that the onset of chlorine activation in the lower stratosphere is caused mainly by liquid-phase sulfate aerosols rather than by NAT particles. A more accurate parameterization of the chlorine activation threshold temperature, T_{ACl}, was derived for varying stratospheric conditions depending on temperature, water

Table 2. Definition of Parameters Used to Derive T_{ACl}

	z = Θ	z = p
α	−4.0628	1.1612
a	480.781	170.216
b	18.569	2.8625
c	0.2711	0.1970
d	6.4481	0.1587
e	1.9915	−0.2457
f	0.05857	0.04705
g	0.2201	0.1665
h	0.07958	0.05914

vapor, and sulfate surface area (K. Drdla, personal communication, 2006):

$$\begin{aligned} T_{ACl} &= a + b \cdot v + c \cdot v^2 + d \cdot s_{e \cdot s^2} + f \cdot s^3 + g \cdot v \cdot s + h \cdot v \cdot s^2 \\ v &= \ln([H_2O] \cdot z^{\alpha}) \\ s &= \ln(SAD), \end{aligned} \quad (1)$$

where z is the vertical coordinate (either potential temperature, Θ, or pressure), $[H_2O]$ is H_2O mixing ratio in ppm, range 1 to 20 ppm, SAD is the sulfate area density at 210 K (μm^2 cm^{-3}), range 0.1 to 100 μm^2 cm^{-3}; the parameters α, a, b, c, d, e, f, g, and h are defined in Table 2. Here, chlorine activation is considered to be efficient if the reactivity exceeds 0.1 d^{-1}. The model of *Carslaw et al.* [1995] was used to calculate the aerosol composition; the model of *Shi et al.* [2001] was used to derive the reactivities of liquid particles. More details about the derivation of this formula will be given elsewhere.

[16] On the basis of this definition, T_{ACl} depends on the H_2O mixing ratio and the surface area density of liquid sulfate. Denitrification and the resulting decrease of HNO_3 does not change the activation temperature. Further, for background conditions, SAD does not influence the chlorine activation temperature significantly. The dependence of changing SAD on the chlorine activation temperature and its impact on chemical ozone loss will be discussed in a different study.

[17] We define the volume of the vortex with temperatures below T_{ACl}, as the volume of potential chlorine activation, V_{ACl}. Accordingly to the PSC formation potential, PFP, we employ a measure that is the fraction of the vortex below the chlorine activation temperature during the ozone hole period. This measure describes the impact of different meteorological conditions on chlorine activation and is defined here as the meteorological part of the potential of activated chlorine, $PACl_{met}$.

[18] However, it is well established that chlorine activation is strongly dependent on the amount of effective stratospheric chlorine [e.g., *Newman et al.*, 2006] in the polar regions. The previously derived diagnostics, V_{PSC}, the potential volume of Polar Stratospheric Cloud (PSC) formation, and PFP, do not depend on EESC. These diagnostics were solely derived for approximately maximum EESC conditions, between 1990 and 2005. Here, we extend these diagnostics and combine the meteorological impact and the impact of changing EESC in a diagnostic to compare to chemical ozone loss. (Our procedure is similar to the one employed by *Brunner et al.* [2006], who considered V_{PSC} * EESC.) The potential for activation of chlorine, PACl, is defined by multiplying $PACl_{met}$ times the normalized $EESC_n$ values for each year, n. $EESC_n$ is EESC values for year n, divided by the maximum of EESC. In this way, PACl is approximately $PACl_{met}$ for the years between 1990 and 2003, when EESC is largest. Using WACCM3 results, we will show a strong correlation between PACl and chlorine activation (see section 5).

[19] Besides the impact of EESC for a long-term analysis, PACl is strongly influenced by different meteorological conditions in the model. To understand the difference between PACl based on model results and based on meteorological analysis, we evaluate temperature conditions in the polar vortex and the sharpness of the polar vortex edge between model results and observations (section 5). Accordingly, V_{ACl}, V_{Vortex}, and the duration of possible ozone depletion, which is the number of days when V_{ACl} is greater than zero, in meteorological analyses and in WACCM3 results are compared.

4.2. Chemical Diagnostics

[20] The performance of chemical ozone loss in the MOZART-3, which constitutes the chemical module of WACCM3, was evaluated in *Kinnison et al.* [2007]. MOZART-3 can be run as an independent chemistry-transport model, using specified meteorological fields. In the study of *Kinnison et al.* [2007], the amount of "active" chlorine in MOZART was found to depend on the transport and the degree of isolation of the vortex for the prescribed meteorological fields. In section 6, the evolution of inorganic chlorine will be discussed based on WACCM3.

[21] The total column of chemical ozone loss is derived using tracer-tracer correlations. In the tracer-tracer correlation method ozone is correlated to a long-lived tracer, for example N_2O, CH_4, or HF. The lifetime of ozone is more than 100 d in the lower stratosphere in the absence of heterogeneous chemistry and so changes of the relation between ozone and a long-lived tracer during the winter can be assumed to be a result of chlorine activation due to heterogeneous chemistry within the polar vortex. This assumption is only valid if the polar vortex is isolated and mixing across the vortex edge can be neglected [e.g., *Proffitt et al.*, 1993; *Plumb et al.*, 2000; *Tilmes et al.*, 2004; *Müller et al.*, 2005]. To obtain chemical ozone loss using tracer-tracer correlations, an early winter reference function has to be derived at a time when the polar vortex is already isolated but before chemical ozone loss has started. Using this relationship between ozone and a long-lived tracer allows us to calculate ozone for chemically unperturbed conditions later in the season, called "proxy ozone." The difference between the proxy ozone and the actually observed ozone describes accumulated chemical ozone loss between the time of the early winter reference function and the time of the observation. Column ozone loss is derived by the integration of the ozone loss profile over a partial column, for example, between 380 and 550 K potential temperature [e.g., *Tilmes et al.*, 2004].

[22] The tracer-tracer correlation technique has been shown to be reliable for calculating chemical ozone loss in polar regions from observations [*Tilmes et al.*, 2004; *Müller et al.*, 2005]. Further, the tracer-tracer correlation method was successfully applied to deduce ozone loss from

climate model simulations [*Lemmen et al.*, 2006b, 2006a]. *Lemmen et al.* [2006b] discussed the application of tracer-tracer correlations to CCMs in detail. Depending on the model used to derive chemical ozone loss, the tracer-tracer correlation technique can have limitations. Numerical diffusion of the model or an insufficiently isolated polar vortex can result in underestimation of chemical ozone loss.

[23] Here, we consider air masses that are located within the polar vortex edge. The polar vortex edge constitutes a transport barrier between midlatitudes and polar regions. *Nash et al.* [1996] have proposed an algorithm where the vortex edge is defined as the maximum of the potential vorticity (PV) gradient constrained by the wind velocity. Additionally, following this algorithm, the location of the local maxima of convex and concave curvature in the PV distribution (with respect to equivalent latitude) defines the poleward and equatorward edges of the vortex boundary region. The area poleward of the inner edge of the vortex boundary region is defined as the ''vortex core.'' The ''entire vortex'' describes the region poleward of the vortex edge, which also includes the vortex core but excludes the equatorward portion of the vortex boundary region. To further distinguish between airmasses of different parts of the vortex, we consider areas of different equivalent latitudes in the model.

5. Meteorology of the Polar Vortices in WACCM3 and Meteorological Analyses

[24] The activation of halogen species in the polar lower stratosphere, and therefore chemical ozone loss, depend strongly on meteorological conditions, especially the temperature prevailing during the polar winter. To understand the reasons for discrepancies in chemical ozone loss between models and observations, meteorological conditions are compared in detail. In this section, the evolution of polar temperatures during the winter, averaged between 1992 and 2002, and the average for the three WACCM3 REF1 realizations is investigated (section 5.1), as well as the spatial temperature distribution within the vortex (section 5.2). Further, the location and strength of the transport barrier of the vortex edge is derived from both model and observations to analyze the size of the vortex and its isolation (section 5.3). Chemical ozone loss may vary significantly depending on these variables. In addition, different meteorological diagnostics are compared between meteorological analyses and WACCM3 results (section 5.4). At the end of this section we compare PACl to the simulated amount of activated chlorine in WACCM3.

5.1. Vortex Average Temperatures

[25] Temperatures between 1992 and 2003, averaged over the entire vortex for the lower stratosphere, from the average of the three WACCM3 model realizations and MetO analyses are shown for Antarctica and the Arctic in Figures 2 and 1, respectively. The potential temperature range of 400 to 600 K shown corresponds to approximately 14 to 25 km in altitude.

[26] In the Arctic, both data sets indicate cooling within the polar vortex between November and March (see Figure 1). For the northern hemisphere between November and January, WACCM3 temperatures are significantly higher (between 2.5 and 10 K) than MetO temperatures between 400 and 600 K (Figure 1, bottom). Therefore MetO minimum temperatures are significantly more often below the activation temperature for chlorine, which results in a significantly different extent of chlorine activation and therefore in different chemical ozone loss between MetO and WACCM3 (as shown below). During February and March both data sets agree within ±2.5 K.

[27] For Antarctica, both WACCM3 and MetO temperatures show decreasing temperatures between May and June and increasing temperatures at the end of September (see Figure 2). Between 450 and 600 K, the WACCM3 temperatures are in good agreement with MetO data, although WACCM3 temperatures are higher by up to 2.5 K in May and by 0–5 K in June, July, and the first half of August. Below 450 K, the temperatures simulated by WACCM3 are lower than MetO data by no more than 2.5 degrees. At the end of August, WACCM3 temperatures develop a cold bias that increases up to 7.5 degrees at the end of September (see Figure 2, dashed lines) when compared to MetO data. As shown in Figure 2, top and middle, WACCM3 temperatures fall below 195 K shortly after MetO temperatures during May. Here 195 K is an approximate threshold temperature for chlorine activation, T_{ACl}, assuming background aerosol conditions (K. Drdla, personal communication, 2006). Further, in both data sets vortex average temperatures stay below 195 K during September and October (not shown here). Between June and September, chlorine activation can be expected based on both WACCM3 and MetO data.

[28] In general, the average temperatures of the entire Arctic and Antarctic vortices between 1992 and 2005 show higher temperatures in the WACCM3 simulations during the first part of the winter and a good agreement during midwinter. At the end of the winter WACCM3 temperatures tend to be lower than MetO data, especially for the Antarctic. The comparison between Antarctic ERA40 temperatures and the WACCM3 model between 1979 and 1999 shows the same result (not shown here). Antarctic ERA40 temperatures show a cold bias compared to MetO data since 1979, described above, but the same temperature evolution during the ozone loss period.

[29] Figure 3 shows Antarctic and Arctic annual vortex temperature of all three WACCM3 realizations between 1960 and 2003. These temperatures were averaged over the entire winter between mid-June and September for Antarctica and between mid-December and March for the Arctic. The ensemble average of WACCM3 is compared to MetO and ERA40. In the Arctic, WACCM3 is biased high by 2–3 degrees when compared to meteorological analyses. In Antarctica, annually averaged temperatures of WACCM3 and MetO data agree very well. This occurs because temperatures are overestimated in WACCM3 at the beginning of each simulated winter and are underestimated at the end of the winter (as described above). In this comparison the low bias of ERA40 data to MetO analyses is also obvious.

[30] In general, the variability of annually averaged temperatures is similar for all three WACCM3 realizations, based on the f-test. The average profile of the ensemble mean is in agreement with meteorological analyses. Additionally, both WACCM3 and observations show a linear temperature trend of ≈ -1 K/(40 years (a)) in the polar

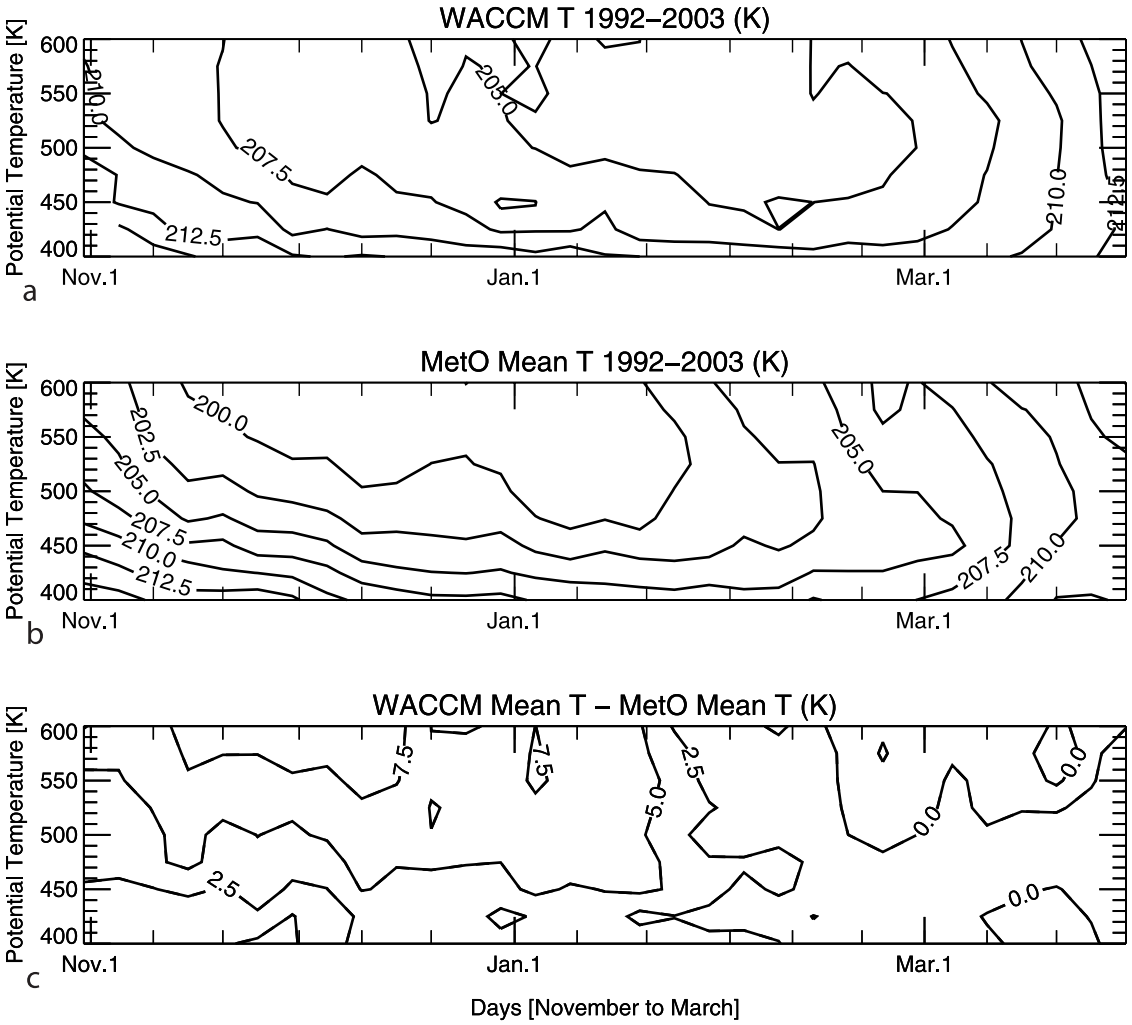

Figure 1. Arctic polar vortex average temperatures between 1992 and 2003 from (a) the WACCM3 simulations and (b) the MetO analysis. Also shown is (c) the difference between MetO analysis and WACCM3 analysis.

vortex in the Arctic. The same trend is calculated for Antarctica in WACCM3 (see Figure 3, straight black and dark gray lines); however, this trend might not be linear due to the radiative impact of the occurrence of the ozone hole in the eighties. This is in agreement with the estimated Antarctic lower stratospheric cooling of approximately 0.25 K decade^{-1} [*IPCC*, 2001]. The changes of Antarctic temperatures from meteorological analyses are not derived because of the rather short period of reliable data.

5.2. Spatial Temperature Distribution Within the Vortex

[31] Investigating the development of vortex average temperatures does not allow us to identify spatial discrepancies between WACCM3 and MetO analysis. However, this is very important to understand the evolution of heterogeneous processes in different regions of the polar vortex. Here we compare the spatial temperature distribution in WACCM3 and MetO analysis with respect to equivalent latitude.

[32] Figures 4a–4d show the temperature distribution averaged between 1992 and 2003 at different equivalent latitudes and two potential temperature surfaces (475 K and 550 K) for the ensemble mean of WACCM3 simulations. Differences between WACCM3 and MetO temperatures are shown in Figures 4e–4h. WACCM3 temperatures (solid lines) are in general slightly higher than observed (up to ≈5 K) equatorward of 50° equivalent latitude. For higher latitudes, differences between model simulations and analyses are seasonally dependent in both hemispheres, which is also noticeable in Figures 1 and 2.

[33] In the beginning of the Arctic winter between November and January, WACCM3 temperatures are ≈5–10 K and up to 5 K higher during February than MetO data (see Figure 4f). During March and April, the WACCM3 and MetO temperatures are in agreement with slightly lower temperatures in the vortex core in April than in March. The average temperature in the Arctic vortex never reach values close to the chlorine activation temperature.

[34] For Antarctica (Figures 4e and 4g), temperatures in the vortex core, poleward of 70°S are in agreement at 550 K potential temperature and slightly colder at 475 K potential temperature between May and July. Starting in August, WACCM3 temperatures tend to be significantly lower than

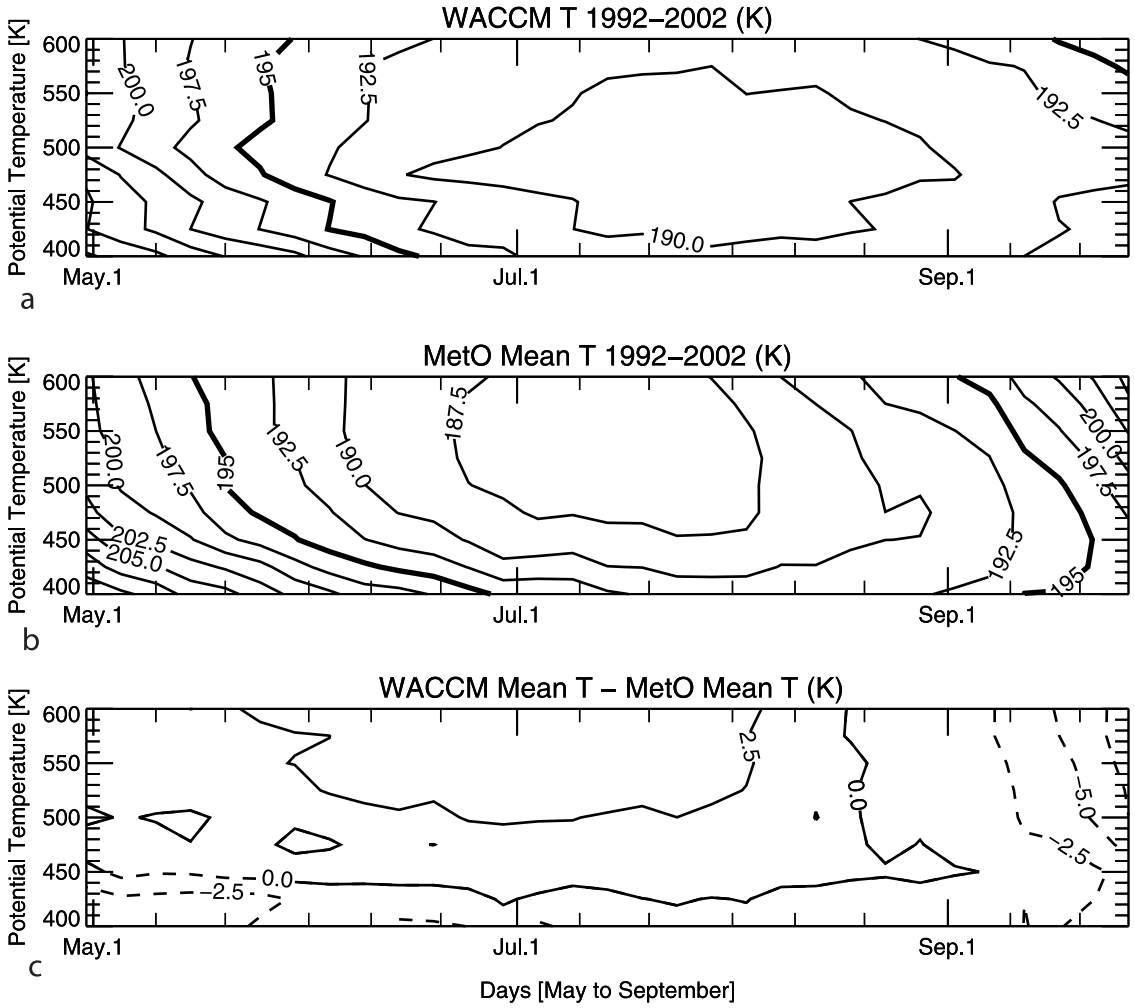

Figure 2. Antarctic polar vortex average temperatures between 1992 and 2003 from (a) the WACCM3 simulations and (b) the MetO analysis. Also shown is (c) the difference between MetO analysis and WACCM3 analysis. Negative values are shown in dashed lines.

MetO temperatures especially during October. Temperatures are in general higher than MetO analyses equatorward of 70°S during the entire period considered. Starting in September, the threshold for chlorine activation of about 195 K is not reached equatorward of ≈70°S. In summary, Antarctic WACCM3 temperatures are higher relative to MetO analysis in the outer region of the polar vortex and cooler within the vortex core. Especially for Antarctica at the end of the winter, there is a significant cold bias in the WACCM3 temperatures compared to MetO analysis for profiles poleward of 70°S.

5.3. Vortex Edge and Vortex Lifetime

[35] To apply tracer-tracer correlation to WACCM3, we need to discuss whether the polar vortex in the model is sufficiently isolated. In this section, the location and strength of the vortex are analysed.

[36] If a vortex edge can be calculated using the algorithm proposed by *Nash et al.* [1996], we assume that the polar vortex exists. During the entire period considered the vortex exists for both WACCM3 simulations and MetO data. To identify the location and strength of the transport barrier between the polar vortex and midlatitudes, we use the the product of the PV gradient with respect to equivalent latitudes and the absolute values of the horizontal wind velocity ($\nabla PV \cdot v$) [e.g., *Bodeker et al.*, 2002; *Tilmes et al.*, 2006b]. Further, *Tilmes et al.* [2006c] estimated a value of 22.8 PVU/degree · m/s for a sufficiently isolated polar vortex. The modified PV is used to compare different altitudes. (A form of potential vorticity that has conservation properties similar to those of Ertel's potential vorticity (EPV) but removes the exponential variation with height displayed by EPV. This form is thus more suitable for inspecting vertical cross sections of potential vorticity and for use (with potential temperature) as a quasi-conserved coordinate in the analysis of chemical constituent data [*Lait*, 1994].) The equivalent latitude at which the maximum $\nabla PV \cdot v$ is reached, which is defined as the location of the vortex edge, differs between different months in model results and meteorological analyses (see Figure 5).

[37] MetO meteorological analyses for the Arctic show an increase of the maximum $\nabla PV \cdot v$ between November and February (Figures 5b and 5d) and thus an increase in the strength of the vortex. The maximum is located between 65° and 68°N. During March, the maximum decreases and

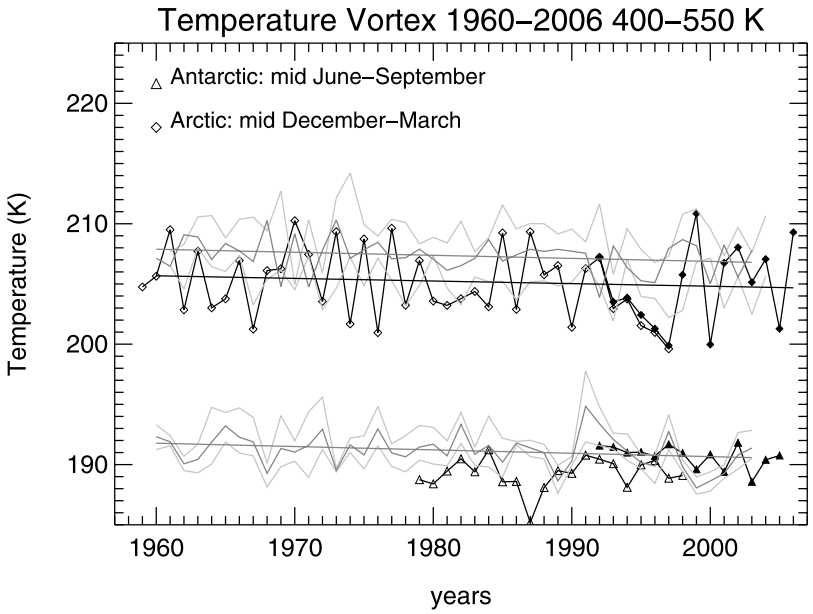

Figure 3. WACCM3 ensemble mean of vortex average temperature in K averaged between 400 and 550 K and between mid-June and September for Antarctic winters and between mid-December and March for Arctic winters (dark gray line). Maximum and minimum variability of the three realizations REF1.1, REF1.2 and REF1.3 are shown as light gray dashed lines. Between 1991 and 2005 UK meteorological analyses (black filled symbols and solid lines) are used and between 1958 (1979 for Antarctica) and 1999 ECMWF reanalysis (ERA40) (black open symbols and solid lines) are used. The WACCM3 trend in 40 years (a) is −1.1 degrees for Antarctica and −1.0 degrees for the Arctic (straight dark gray lines). The trend in 40 a for meteorological analysis for the Arctic is −0.9 degrees (straight black line).

moves poleward toward 70°N. Starting in April, no significant maximum $\nabla PV \cdot v$ can be found. The polar vortex becomes stronger between November and February and becomes weaker thereafter. In comparison, the maximum $\nabla PV \cdot v$ of the WACCM3 simulations is smaller and located further poleward (between 70° and 80°N) with a much wider peak compared to the analysis. Therefore the area of the Arctic polar vortex is smaller in the WACCM3 simulations than in the observations. The largest maximum occurs in March. In April the vortex becomes weaker in the model simulations, in agreement with meteorological analyses. For all months the WACCM3 maximum $\nabla PV \cdot v$ values are significantly smaller (less than 20 PVU/degree · m/s) at 475 K and about half at 550 K compared to the MetO analysis. The estimated value of 22.8 PVU/degree · m/s for an isolated polar vortex [*Tilmes et al.*, 2006b] is not reached at the 475 K potential temperature level in WACCM3. At 550 K the polar vortex is less isolated between January and March, applying the same criterion. Only during November is the maximum $\nabla PV \cdot v$ larger in the model simulations. The wider and lower peak indicates a smaller well-mixed homogeneous area within the vortex compared to the analysis and a less isolated vortex than using MetO data. The lifetime of the Arctic vortex in the WACCM3 simulations is in agreement with the analyses. To explain the reason for the rather small vortex area in WACCM3 is beyond the scope of this paper and will be a subject of a further study.

[38] For Antarctica the MetO maximum $\nabla PV \cdot v$ increases over the period between June and September and is still rather large during October at both altitudes considered (Figures 5a and 5c). The maximum is located between 65 and 70°S equivalent latitude. The peak of the maximum $\nabla PV \cdot v$ in Antarctica is approximately as wide as for the Arctic in the meteorological analyses. WACCM3 simulations show a smaller value of the maximum $\nabla PV \cdot v$ in Antarctica between August and October at 475 K and similar values at 550 K. The wider peak of the maximum developed in WACCM3 for all months, especially between August and October, is more pronounced at 475 K. In general, the Antarctic polar vortex seems to be less isolated in the WACCM3 simulations than in MetO data. Further, the peak of the distribution of $\nabla PV \cdot v$ is much wider and the maximum of $\nabla PV \cdot v$ is located further equatorward between July and September than in the MetO analyses. As a result, the area of the entire Antarctic polar vortex in WACCM3 is larger than in the MetO analysis during this period.

5.4. Potential for Activation of Chlorine (PACl) in WACCM3

[39] Using WACCM3 simulations, the ensemble mean of V_{ACl}, defined in section 4.1, is calculated (Figure 6a, dark grey line). We calculated the threshold temperature for chlorine activation for WACCM3 results using equation (1) and using gas phase H_2O and SAD from the WACCM3 simulations. Further, the volume of the entire vortex, the activation time and meteorological part of the potential of activated chlorine $PACl_{met}$, as defined in section 4.1, were derived (Figures 6b, 6c, and 6d).

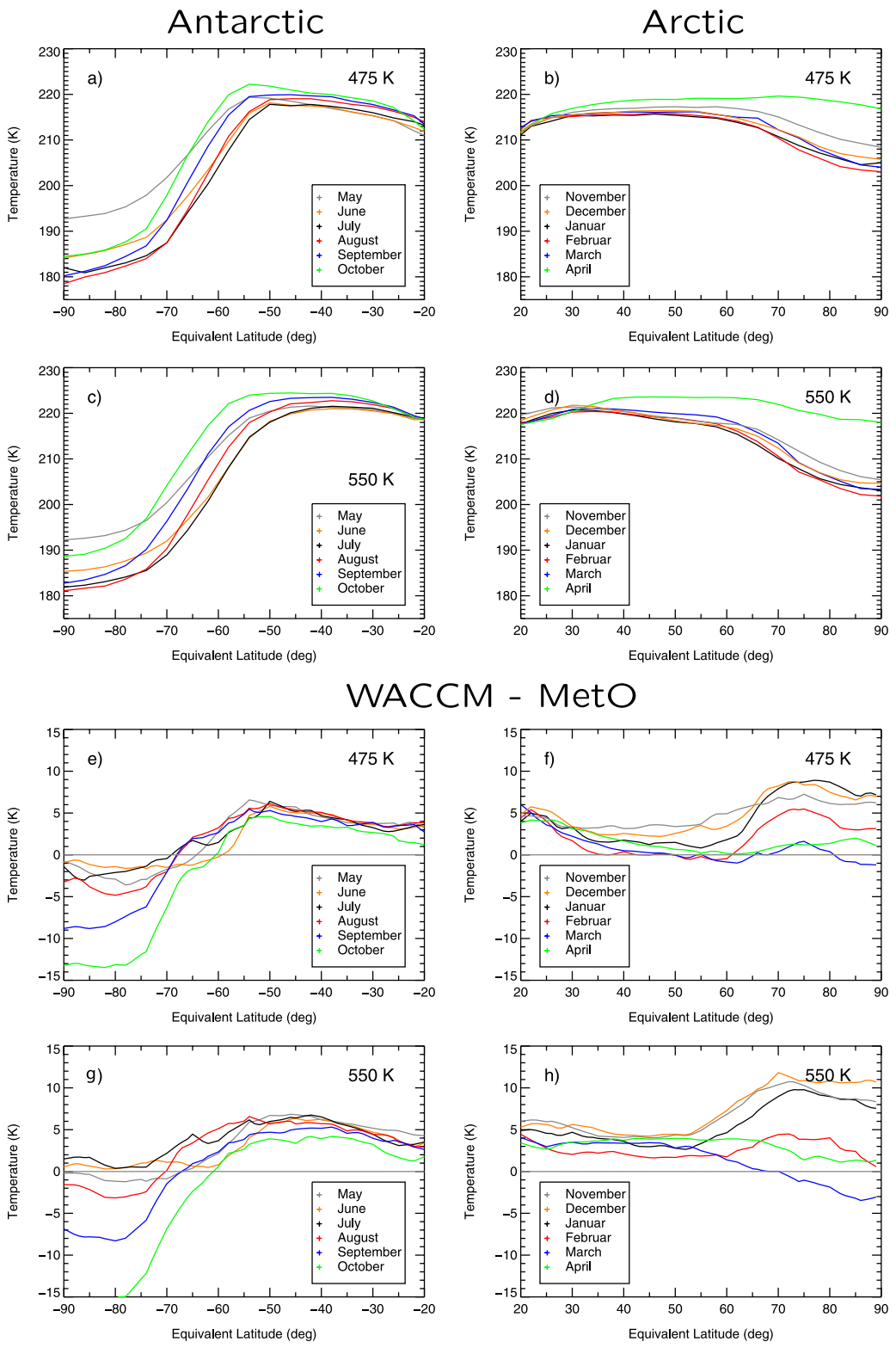

Figure 4. WACCM3 averaged temperature distribution with respect to equivalent latitude between 1992 and 2003 for different months (different colors) at (a,b) 475 K potential temperature and at (c,d) 550 K potential temperature. Also shown are differences between WACCM3 and MetO (e,f) at 475 K potential temperature and (g,h) at 550 K potential temperature. Left column illustrates the southern hemisphere and right column illustrates the northern hemisphere.

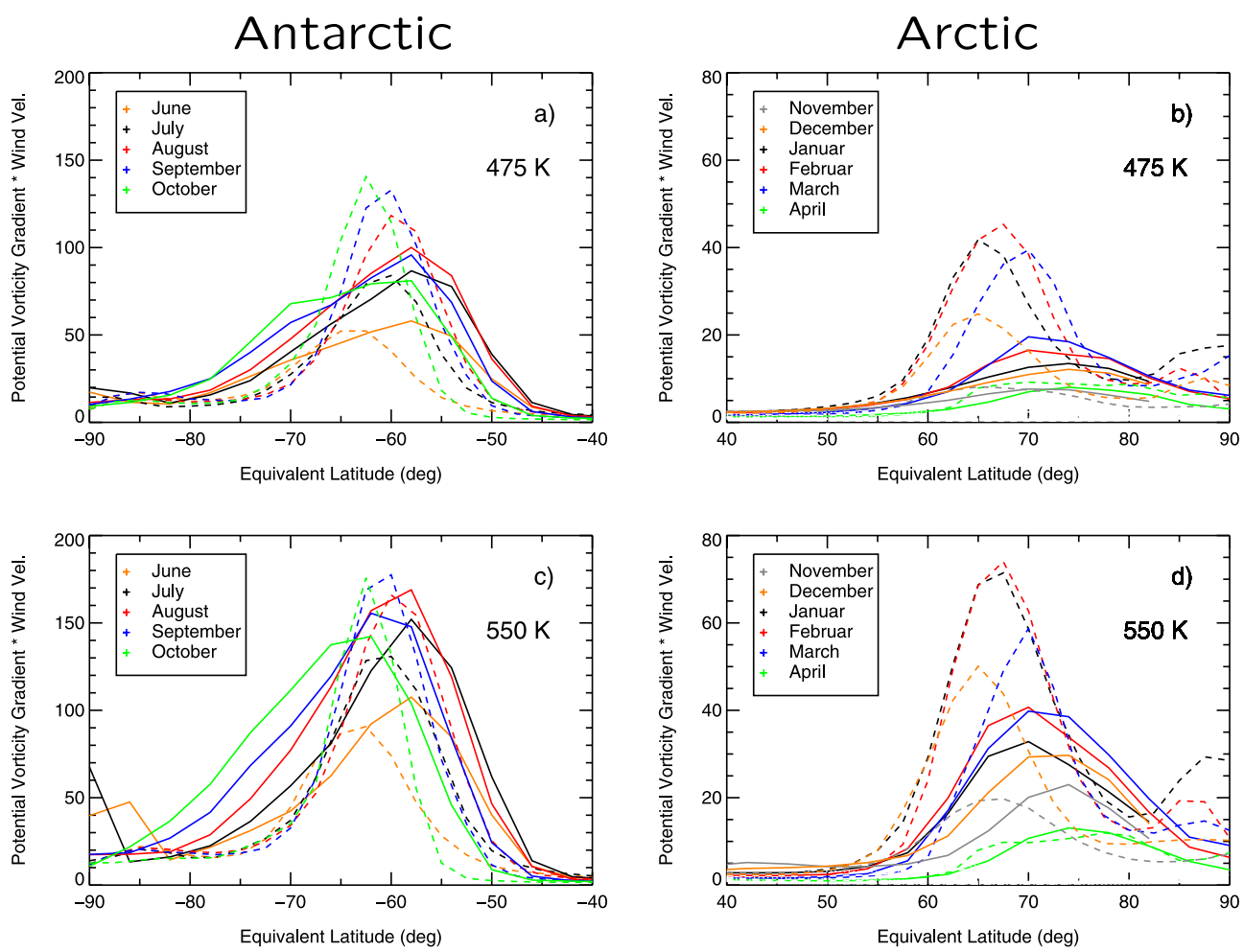

Figure 5. Gradient of modified Potential Vorticity (PV) (see text) times wind velocity with respect to equivalent latitude between 1992 and 2003 for different months (different colors) (a,b) at 475 K potential temperature and (c,d) at 550 K potential temperature. WACCM3 model simulations are shown as solid lines and MetO analysis are shown as dashed lines. Left column illustrates the southern hemisphere and right column illustrates the northern hemisphere.

[40] We compare these diagnostics derived using WACCM3 to meteorological analyses between 1991 and 2006 using MetO data and between 1958 (1979 for Antarctica) and 1999 using ERA40 data (filled symbols and black solid lines). For the calculation of T_{ACl} using meteorological analyses, the monthly averaged SAD data set is used that was produced by the Assessment of Stratospheric Aerosol Properties (ASAP) based on gridded SAGE II observations [*Thomason and Peter*, 2006].

[41] In the Arctic, temperatures in the WACCM3 simulations are higher than in meteorological analyses, which results in smaller V_{ACl}. However, some simulated Arctic winters reach V_{ACl} values that are comparable to moderately cold observed winters (light gray lines in Figure 6a). Nevertheless, temperatures of observed climatologically cold winters, as in 2000 and 2005, are not reached in the WACCM3 simulations. The characteristics of a cold WACCM Arctic winter (year 2001), in one WACCM3 realization, will be compared below to an observed climatologically cold Arctic winter below. WACCM3 V_{ACl} increases by and 0.2×10^7 km^3 over 40 a. Meteorological analysis show an increase of 0.9×10^7 km^3 for the Arctic. The reason for the smaller increase of WACCM3 V_{ACl} during this period is that WACCM3 temperatures in the Arctic do not reach the threshold value for chlorine activation as often as meteorological analyses. Further, volume of the Arctic vortex is underestimated in WACCM3, because the edge of the simulated Arctic vortex is located further poleward compared to meteorological data. Neither WACCM3 results nor meteorological analysis show a significant trend. $PACl_{met}$ for the Arctic is significantly smaller than meteorological analyses, even for cold simulated winters (see Figure 6d). This happens because the simulated low temperatures in the vortex are present during a much shorter (about half) activation period compared to observations as shown in Figure 6c.

[42] For Antarctica, the V_{ACl} calculated using results from WACCM3 for all three realizations, agrees well with meteorological analyses (Figure 6a). The variability of V_{ACl} for all three WACCM3 realizations is somewhat larger than for the meteorological analyses (light gray dashed lines). WACCM3 V_{ACl} increases by 1.5×10^7 km^3 for Antarctica

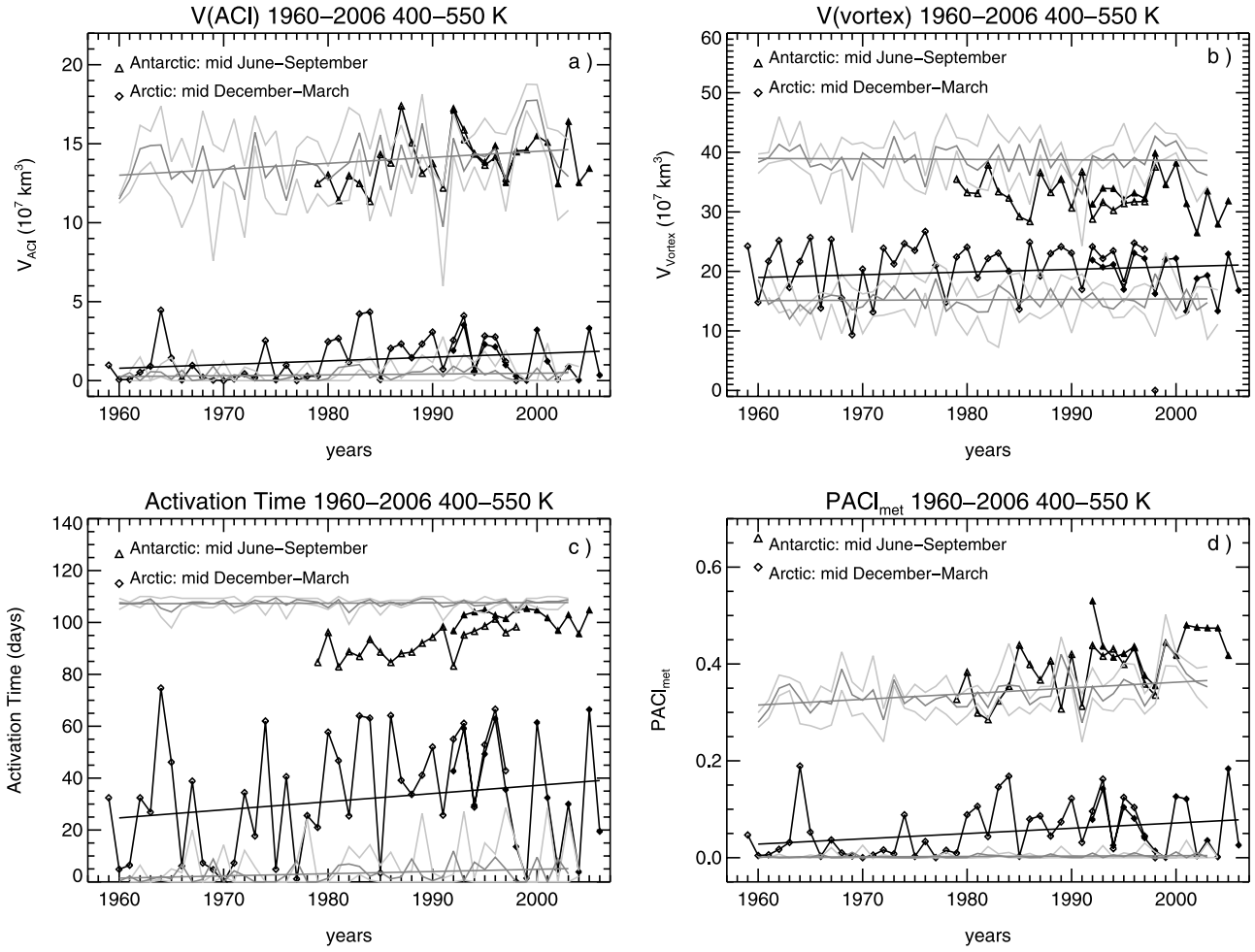

Figure 6. WACCM3 ensemble mean of (a) the volume of possible chlorine activation, V_{ACl}, in 10^7 km^3, (b) volume of the polar vortex, V_{vortex}, (c) the activation time in days, and (d) the meteorological part of the potential of activated chlorine, $PACl_{met}$ (see text), averaged between 400 and 550 K and between mid-June and September for Antarctic winters and between mid-December and March for Arctic winters (dark gray line). Maximum and minimum variability of all three realizations, REF1.1, REF1.2, and REF1.3 are shown as light gray lines. Between 1991 and 2006 MetO analyses (filled black symbols and solid lines) are used and between 1958 (1979 for Antarctica) and 1999 ECMWF reanalysis (ERA40) (open black symbols and solid lines) are used. The straight dark gray line indicates the trend of all three WACCM3 realizations and the straight black line the trend of meteorological analysis. For the Antarctic no trend was calculated because of the shorter period of data.

over 40 a. The WACCM3 Antarctic vortex volume is larger compared to meteorological analyses for most winters (Figure 6b). As described in section 5.3, the edge of the Antarctic polar vortex, relative to meteorological analyses, is located toward lower latitudes and does not show a significant trend. A decreasing vortex volume during the last decade for Antarctica was described by *Tilmes et al.* [2006a]. The resulting larger volume of the simulated Antarctic vortex and slightly larger V_{ACl} result in similar $PACl_{met}$ values in WACCM3 and meteorological analyses. However, MetO analysis show larger $PACl_{met}$ for the last 5 a. $PACl_{met}$ decreases by 0.047 (about 3–4%) in 40 a in WACCM3 for Antarctica.

[43] Considering the evolution of $PACl_{met}$ in 40 a, WACCM3 and the meteorological analyses show an increasing trend of $PACl_{met}$ in both Arctic and Antarctic. This is a result of decreasing temperatures in the polar vortex in 40 a. However, from this statistic it is not clear whether this temperature decrease is the result of the occurrence of significant ozone destruction since the 1980s or the result of increasing greenhouse gases in the atmosphere or a combination of both factors. A similar trend for the Arctic and Antarctica indicates that the increase of greenhouse gases is a possible factor driving the decrease of polar temperatures because the entire column ozone in the Arctic did not change as drastically as in Antarctica.

[44] PACl, including the impact of changing ozone destroying substances in the atmosphere (defined in section 4.1) is shown in Figure 7. In comparison to $PACl_{met}$ (black dashed line), PACl (red dashed line) is strongly correlated (correlation coefficient >0.9) to the ''activated'' halogen loading in the Antarctic polar vortex based on model results.

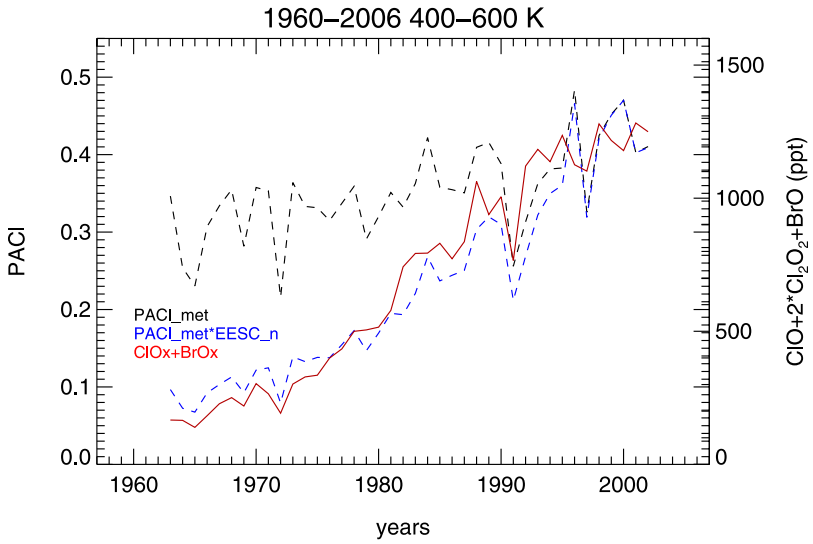

Figure 7. Meteorological part of the potential of activated chlorine, $PACl_{met}$ (black dashed line), PACl including the effective chlorine loading in the stratosphere (black dashed line), and the sum of activated chlorine ClO_x and bromine BrO_x compounds within the Antarctic polar vortex, averaged between mid-June and September and between 400 and 600 K.

We conclude that PACl is an appropriate diagnostic for comparing with the halogen activation in the model, and therefore for chemical ozone loss. The impact of changing EESC in the stratosphere on chemical ozone loss between 1960 and 2003 is therefore taken into account when considering the relationship between chemical ozone loss and PACl (see section 7).

6. Heterogeneous Processes and Chemical Ozone Loss in WACCM3 and Observations

[45] The meteorological situation in WACCM3 has an impact on chemical processes in the model. In this section, heterogeneous processes in the model are described. The evolution of activated chlorine compounds ClO_x = Cl + $2Cl_2$ + ClO + OClO + $2Cl_2O_2$ + HOCl) and inorganic chlorine reservoir species (HCl and $ClONO_2$), as well as other species in the model for both hemispheres are discussed. Further, chemical ozone loss derived using tracer-tracer correlations will be discussed based on the example of a single observed winter and for all winters between 1960 and 2003 in WACCM3.

6.1. Chlorine Activation in the Polar Vortex During a Specific Arctic and Antarctic Winter

[46] The evolution of different species for one Antarctic and a cold Arctic winter in WACCM3 at the 475 K potential temperature level, is shown in Figure 8. First, we describe the evolution of descent in the model to differentiate between chemical and transport processes for different species. For this, we consider the evolution of the long-lived tracer N_2O (see Figure 8, first row).

[47] In the Antarctic, strongest descent has already taken place between March and May in WACCM3 (not shown). Some descent still occurs between May and August in the outer part of the vortex (black line). Temperatures in this region are warmer in early winter.

[48] For the Antarctic poleward of 70°S, the strong decrease of ozone mixing ratios is a result of chemical ozone destruction. The evolution of ozone mixing ratios during the Antarctic winter is explained next. From May on, chlorine reservoirs in the Antarctic are activated. In particular, $ClONO_2$ decreases markedly with increasing ClO_x mixing ratios (compare Figure 8, left column, third and fifth row). During May and June, "activated chlorine" is not yet photolyzed and thus in the form of Cl_2. However, as soon as airmasses are exposed to some sunlight, chlorine molecules photolyze and the "activated chlorine" is dominated by ClO and its dimer, Cl_2O_2. Catalytic ozone loss cycles occur. Starting in June, WACCM3 model results show increasing mixing ratios of the ClO_x. However, very little sunlight reaches the polar vortex at this time and ClO mixing ratios are almost zero until July.

[49] Beginning in July, ClO mixing ratios between 60–80°S increase slowly. Accordingly, ozone mixing ratios slowly decrease due to ozone depletion by ClO_x and BrO_x chemical families. It should be noted that the ClO values shown here are averaged over day and night regions of the vortex. Daylight maximum ClO mixing ratios in WACCM3 reach up to 2 ppbv in the polar vortex beginning in July (not shown) and are in agreement with MLS ClO measurements [cf. *WMO*, 2007, Figures 4–10]. In the outer part of the vortex, equatorward of 70°S, activated chlorine is much smaller and chlorine activation starts later. This is a result of higher temperatures in this region of the vortex (see Figure 8, bottom row). Further, chlorine reservoirs, especially $ClONO_2$, do not decrease very much. During August, chlorine activation decreases rapidly in this part of the vortex. Accordingly, the chlorine reservoirs, $ClONO_2$ and HCl, increase and ozone mixing ratios do not decrease much further. At that time, the vortex region equatorward of 70°S in WACCM3 is too warm for further chlorine activation and the deactivation process starts.

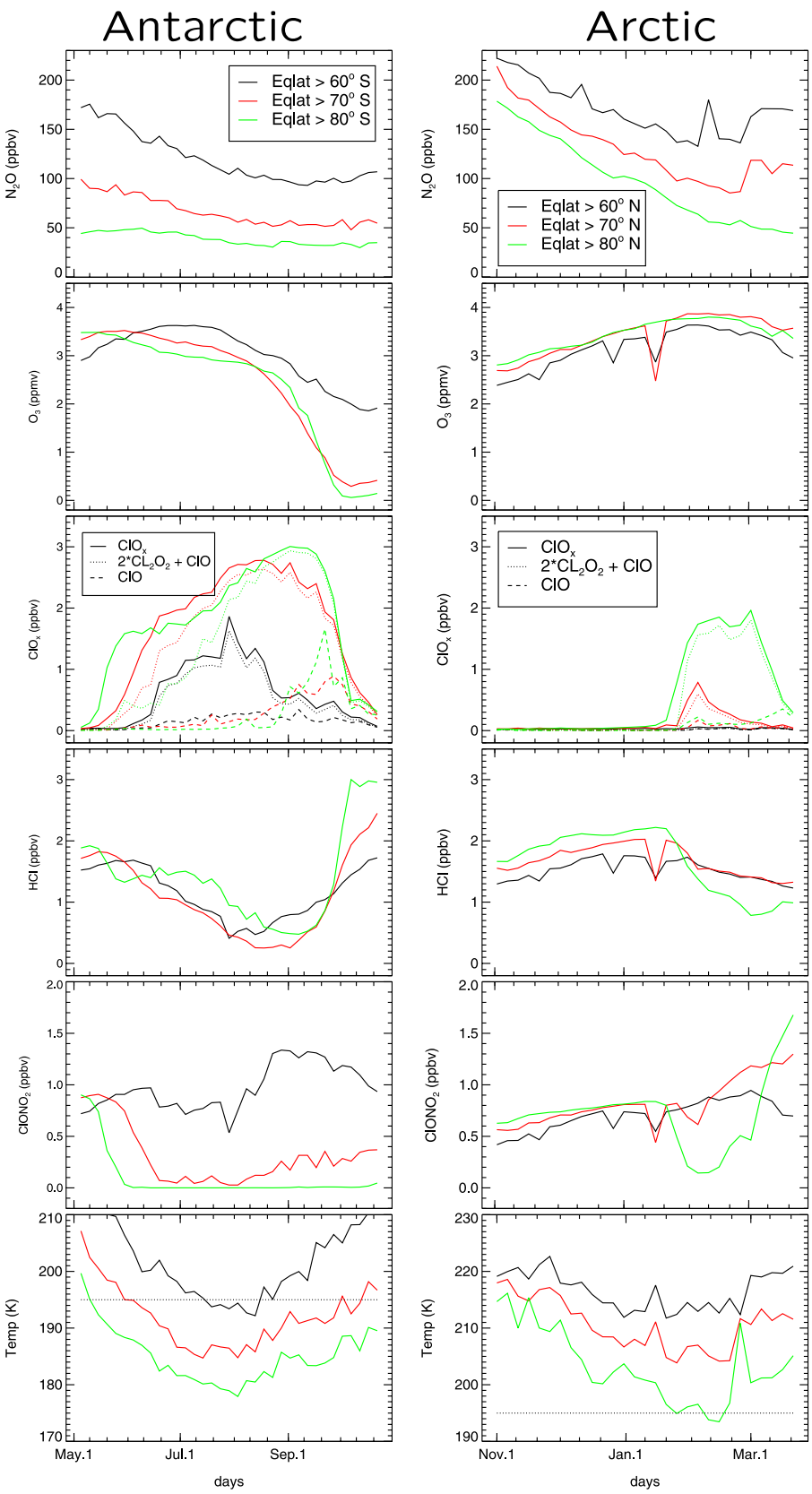

Figure 8. Evolution of different species and temperature in the polar vortex during the ozone loss season in Antarctica and Arctic using the REF1.3 WACCM3 realization for the winter 2000 and 2000–2001, respectively. Different colors indicate different equivalent latitude regions of the results. Beside activated chlorine (third row) additionally the evolution of 2 × Cl_2O_2 + ClO (dotted line) and of ClO (dashed line) is shown.

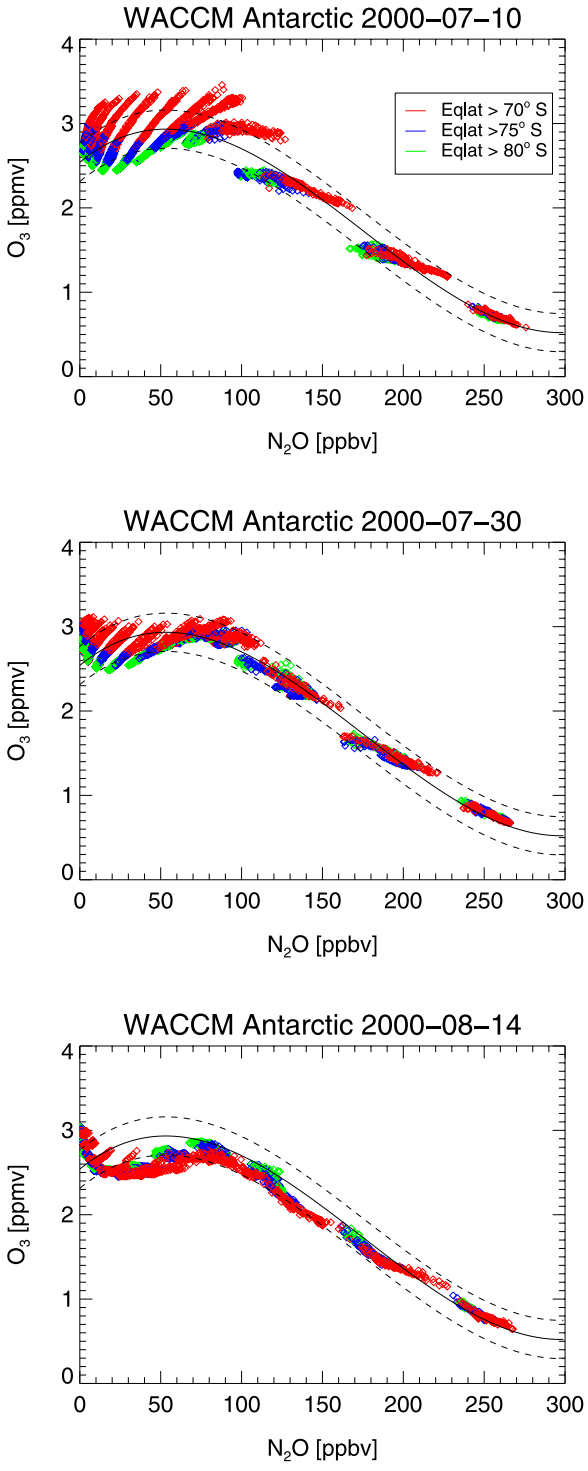

Figure 9. O_3/N_2O tracer relations for three different time intervals using the REF1.3 WACCM3 realization for the winter 2000 shown for three different equivalent latitudes (red: 70–75°S; blue: 75–80°S; green: 80–90°S) within the Antarctic polar vortex. The early winter reference function (solid line) and the uncertainty (dashed lines) shown in each interval were derived for profile in the beginning of July (top).

[50] Poleward of 70°S, during September, the fraction of ClO compared to Cl_2O_2 increases with increasing illumination as expected. At that time, ozone is destroyed rapidly up to the end of September poleward of 80°S. The decrease of ozone mixing ratios poleward of 80°S is in agreement with ILAS-II observations [*Tilmes et al.*, 2006c], as further discussed later. For conditions of low ozone and low NO_x (as occur in Antarctica in spring) after severe ozone depletion, the Cl/ClO ratio is very high. Chlorine deactivation proceeds via $Cl + CH_4 \rightarrow HCl + CH_3$. Under such circumstances HCl increases by more than a factor of two within days reaching values of up to 2.7 ppbv [*Douglas et al.*, 1995; *Grooß et al.*, 1997], as can be seen in WACCM3. Deactivation into $ClONO_2$ cannot be important because earlier denitrification has removed the necessary nitrogen. In the region between 70 and 80°S, deactivation is already obvious at the beginning of September, due to too warm temperatures at this time. In contrast to regions further poleward, $ClONO_2$ is slowly increasing. The differences between different vortex regions are a result of the inhomogeneous nature of the polar vortex in the model, as discussed below.

[51] For the Arctic, the evolution of N_2O indicates strongest descent in the vortex core, as expected. As described above, the Arctic vortex edge is located around 70°N in WACCM3. Therefore, the outer part of the Arctic vortex is influenced by air from outside the vortex, as indicated by the significantly higher N_2O ratios. Ozone mixing ratios increase where descent occurs, since, at the altitude considered, ozone mixing ratios increase with altitudes (see Figure 8, second row). Temperatures within the Arctic polar vortex are above the activation temperature for most of the winter (see Figure 8, right column, bottom row). During February and March, some chlorine is activated, mainly north of 80°S and a slight decrease of the reservoir species can be recognized. However, ClO mixing ratios stay always very low and do not allow ozone loss values comparable to those observed for cold Arctic winters.

6.2. Tracer-Tracer Correlations Applied to WACCM3

[52] In this section, chemical ozone loss based on the three realizations of WACCM3 is derived using tracer-tracer correlations. The results are compared with measurements by ILAS-II for the 2003 Antarctic winter and by HALOE between 1992 and 2004. N_2O is used as the long-lived tracer. An early winter reference function, here O_3/N_2O, has to be derived. Assuming homogeneous tracer distributions within the polar vortex, a compact relationship should be available at the beginning of the winter. Figure 9 shows O_3/N_2O correlations at the beginning of the Antarctic winter 2001 in the WACCM3 REF1.3 run.

[53] In mid-July, the Antarctic polar vortex in the WACCM3 simulations exists and the transport barrier is as strong as shown in MetO (see Figure 5). We derive an early winter reference function, valid for profiles in the beginning of July between 70–90°S equivalent latitude (Figure 9, top, solid line). The uncertainty (defined as the standard deviation of the profiles incorporated in the reference function) is shown as dashed lines. However, the relationship between ozone and N_2O of all profiles inside the polar vortex in WACCM3 is not as compact as observed

in the beginning of July (see Figure 9, top). Ozone and N_2O mixing ratios are slightly smaller for equivalent latitudes poleward of 80°S than for equivalent latitudes further outside the vortex. To calculate chemical ozone loss, we will take this offset of profiles from the reference function of different equivalent latitude intervals into account.

[54] By late July, profiles between 70 and 75°S show a decrease of ozone mixing ratios, which indicates chemical ozone loss in the outer vortex at this time of the year, as seen in Figure 9, middle. Ozone loss at all equivalent latitudes between 65 and 90°S does not start before the beginning of August, 2 weeks later than derived in the Antarctic winter, 2003, using ILAS-II observations. Regions at equivalent latitudes poleward of 70°S, are seldom illuminated before August because the Antarctic vortex in WACCM3 is not significantly displaced from the pole in July, as can be seen in observations. Therefore less ozone loss can occur at this time of the year in WACCM3 than in observations and early chemical ozone loss in WACCM3 is underestimated. Starting in mid-August, all profiles within the entire vortex are homogeneously distributed and occur below the reference function between 70 and 90°S (Figure 9, bottom). The evolution of chemical ozone loss from August on is discussed in section 6.3. The uncertainty of chemical ozone loss derived from the reference function is ≈15 DU.

[55] An inhomogeneous distribution of tracers within the entire polar vortex in WACCM3 also occurs later in the winter between August and October, as shown in Figure 10. Simulated O_3, N_2O, H_2O, and HNO_3 mixing ratios are well mixed within the vortex core (poleward of about 75°S) with slightly smaller mixing ratios in the center of the vortex. This indicates a strong mixing barrier equatorward of the polar vortex core between August and October and a homogeneously distributed vortex center. Equatorward of 75°S, although still inside the polar vortex edge, species are inhomogeneously distributed; for example, N_2O mixing ratios steadily increases between the vortex core and the vortex edge. Further, H_2O mixing ratios are very low within the vortex core. During the Antarctic winter, H_2O was absorbed to form ice particles, because temperatures in this region are below 185 K (see Figure 8, left). Permanent dehydration due to the fallout of these ice particles has occurred in the polar vortex core. The inhomogeneous distribution of species outside the vortex core is a result of the wide area of the polar vortex edge (indicated in the wide maximum of the PV gradient, as described in section 5.3). This wide maximum of the PV gradient is located between 65°S and 80°S and results in a transport barrier that does not allow air masses to mix in different equivalent latitudes bands. A well-mixed entire polar vortex cannot develop.

[56] Figure 11 shows O_3/N_2O correlations at the beginning of the coldest Arctic winter simulated by WACCM3. The O_3/N_2O correlations are compact during mid-December (Figure 11, top) and no profiles are found equatorward of 70°N because the vortex edge is located at ≈70°N, as shown above. Between December and January, the correlation changes towards larger ozone and N_2O mixing ratios (Figure 11, middle). Here, isentropic mixing across the vortex edge is possible because the vortex edge in WACCM3 is very weak, see Figure 5. As a result, tracer-tracer correlations still change between December and January (ozone increases relative to N_2O) and the early winter reference function can only be derived after mid-January. Besides, no ozone loss is expected to occur before mid-January in WACCM3 because the vortex area is not illuminated at that time of the year, Figure 8, right. A similar increase of ozone mixing ratios in the ozone-tracer relationship between November and January was observed for the Arctic winter 1996–1997, based on ILAS satellite observations [*Tilmes et al.*, 2003] as a result of a weak early polar vortex.

[57] During the entire Arctic winter, O_3, N_2O, and H_2O do not change significantly, as shown in Figure 12. HNO_3 mixing ratios show a significant decrease in the entire vortex region and smaller values within the vortex core. All the species are homogeneously distributed within the polar vortex core. Although the Arctic vortex edge is weaker than observed, as shown in section 5.3, the entire vortex does not seem to be strongly influenced by mixing processes; no further increase of the O_3/N_2O relation occurred in mid-January. Therefore the tracer-tracer correlation technique can be applied to this model to calculate chemical ozone loss in the polar vortex core. Later, in the beginning of February, there is still no change of the WACCM3 tracer-tracer correlations. The cold part of the WACCM3 Arctic vortex is not illuminated by the sun and chemical ozone loss cannot be expected in the model. At the end of March, ozone-tracer relations show only minor deviations from the early winter reference function within the core of the polar vortex for one particular cold winter (not shown).

6.3. Temporal Evolution of Antarctic Chemical Ozone Loss

[58] In this section the temporal evolution of Antarctic chemical ozone loss of the WACCM3 model is compared to ILAS-II observations [*Tilmes et al.*, 2006c]. O_3/N_2O correlations for approximately equal time intervals are divided into different equivalent latitudes (see Figure 13, colored profiles). An early winter reference function was derived for the first half of July for the observations [*Tilmes et al.*, 2006c] and model results. The early start of chemical ozone loss during July in the outer part of the vortex was discussed above (as shown in Figure 9). Here, we focus on the evolution of chemical ozone loss between August and October in both model and observations.

[59] During the end of August and the beginning of September ILAS-II data show the largest variability of profiles in the entire vortex during the winter. Largest deviations from the early winter reference function occur in lower latitudes (between 70°S and 80°S). Here, ozone destruction is favored due to a larger amount of sunlight than at very high latitudes [*Tilmes et al.*, 2006c]. The WACCM3 O_3/N_2O relationship is more compact than observed (Figure 13, red, blue, and green profiles). Nevertheless, slightly larger deviations occur between 70 and 80°S than poleward of 80°S (see Figure 13, green profiles) in agreement with observations. A smaller decrease of tracer-tracer correlations between mid-August and mid-September in WACCM3 than in observations is the result of the smaller displacement of the WACCM3 Antarctic

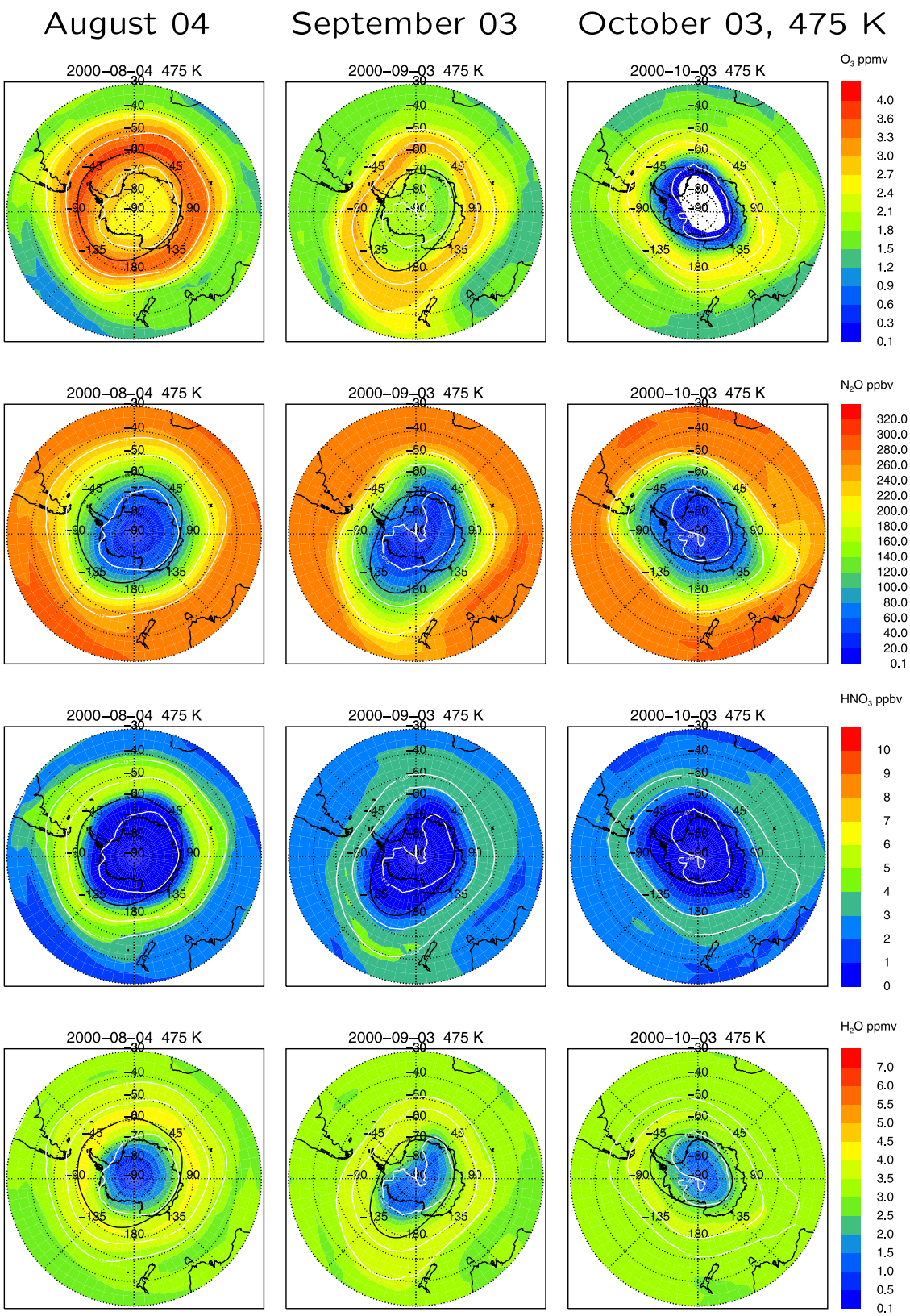

Figure 10. Distribution of different species, O_3 (first row), N_2O (second row), HNO_3 (third row), and H_2O (fourth row) in the Antarctic polar vortex on the 475 K isentropic surface for different days of one WACCM3 realization. White lines indicate the poleward edge, the edge, and the equatorward edge of the polar vortex; see section 3. The black line indicates the area below 195 K, the approximate temperature threshold for chlorine activation.

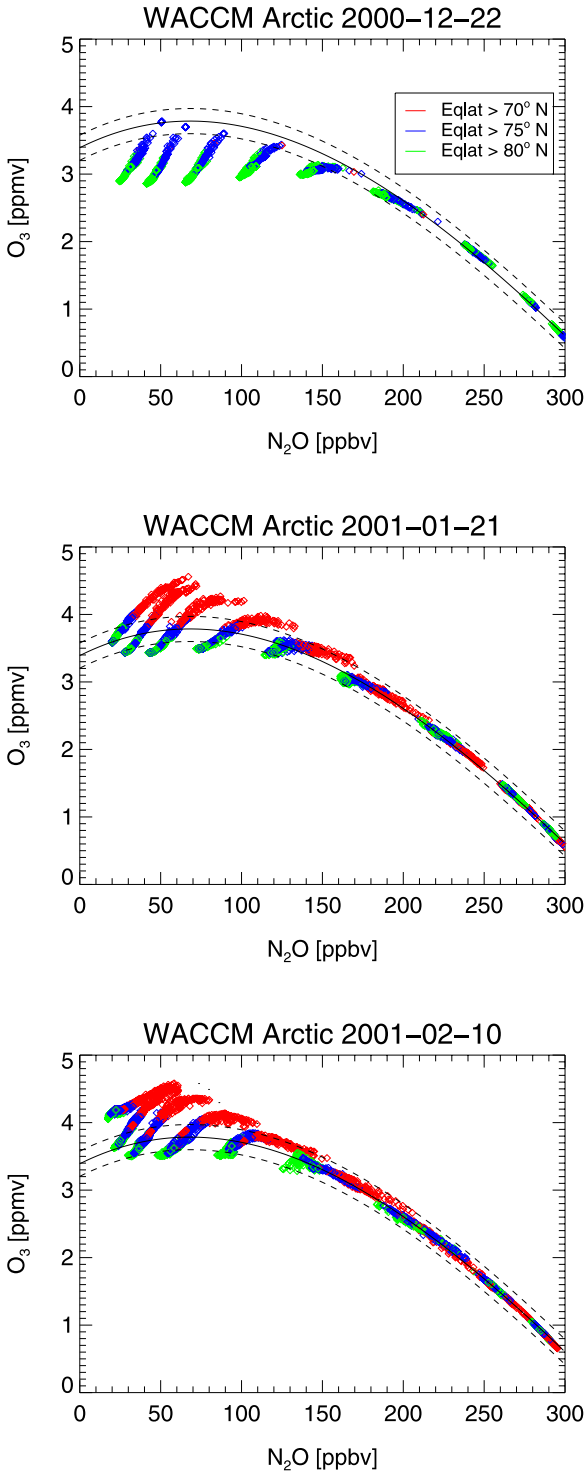

Figure 11. O_3/N_2O tracer relations for three different time intervals using one WACCM3 realization third in winter 2001 for different equivalent latitudes (red: 70–75°S; blue: 75–80°S; green: 80–90°S) within the Arctic polar vortex. The early winter reference function (solid line) and the uncertainty (dashed lines) were derived on 21 January (middle) and are shown in all three intervals.

polar vortex towards illuminated regions for different equivalent latitudes.

[60] During the second part of September, ILAS-II observations already show very low ozone mixing ratios, especially poleward of 80°S. WACCM3 tracer-tracer correlations are compact between 75 and 90°S (green and blue symbols). WACCM3 profiles equatorward of 75°S show partly a less strong deviation from the early winter reference function at the beginning of October. WACCM3 ozone mixing ratios within the vortex edge range between almost zero at the core and much greater values that show less chemical ozone loss, at the edge of the vortex (see Figure 14). As discussed above in Figure 8, at this time the deactivation processes in WACCM3 is already completed in the outer region of the polar vortex and chemical ozone depletion has stopped.

[61] The inhomogeneous distribution of WACCM3 O_3 and N_2O mixing ratios equatorward 75°S, as shown in Figure 14, red symbols, results in an inhomogeneous tracer-tracer correlation (see Figure 13). Outside the vortex core, model results scatter toward larger ozone mixing ratios and therefore toward the early winter reference function. Therefore chemical ozone loss is on average less in the outer region than inside the vortex core, as shown in the following.

[62] The evolution of vortex averaged chemical ozone loss for different equivalent latitudes in WACCM3 is compared to ILAS-II results derived by *Tilmes et al.* [2006c] (see Figure 15). Beginning from August, WACCM3 chemical ozone loss for the three different latitude intervals, 70–75°S, 75–80°S, and 80–90°S, is in good agreement with ILAS-II ozone loss averaged over equivalent latitudes between 65 and 90°S (see Figure 15, top). Ozone loss in the region of the vortex between 70 and 75°S increases faster than in the vortex core until mid-September (red line in Figure 15, top, in agreement with a larger amount of sunlight reaching the outer part of the polar vortex, as described above. Starting in mid-September, ozone loss between 70 and 75°S is less rapid compared to regions further poleward and chlorine deactivation has started.

[63] The outer part of the vortex, between 65 and 70°S (Figure 15, top, black line) chemical ozone loss decreases rapidly during September. Only half of the entire ozone loss is reached in October, due to the warm temperatures in this region of the vortex in the model. Therefore chemical ozone loss derived for the entire vortex in WACCM3, between 65 and 90°S equivalent latitudes is underestimated, see Figure 15, bottom.

[64] For regions between 70 and 90°S, the evolution of chemical ozone loss is in good agreement with ILAS-II observations. The slope of the curve describing accumulated chemical ozone loss is very similar for both the model simulations and the observations. Therefore chemical ozone loss rates in the vortex core can be reproduced by WACCM3 for Antarctica during August and September. For the entire vortex, chemical ozone loss is smaller by one third due to the inhomogeneous distribution of ozone loss in the entire vortex.

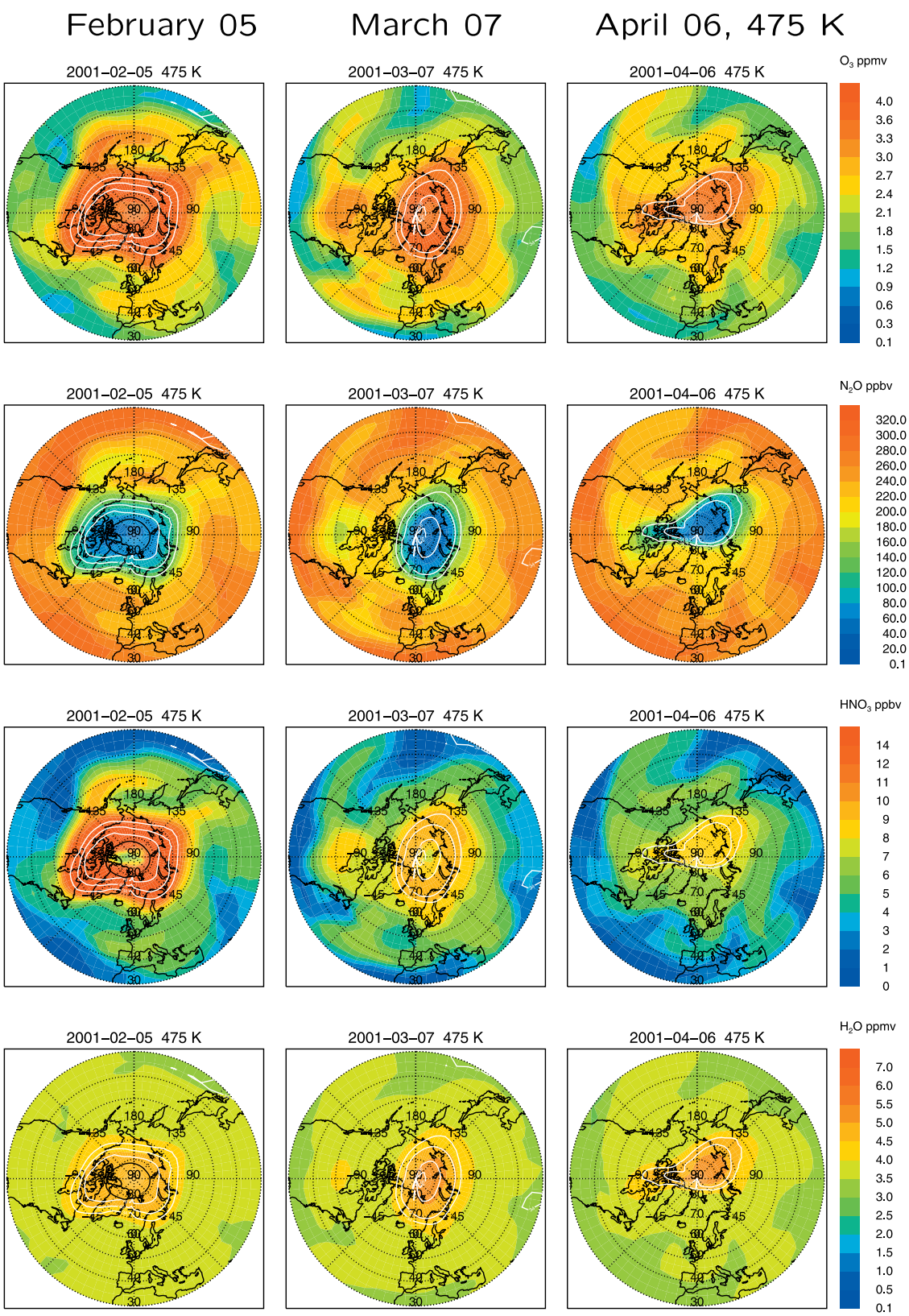

Figure 12. Distribution of different species, O_3 (first row), N_2O (second row), HNO_3 (third row), and H_2O (fourth row) in the Antarctic polar vortex on the 475 K isentropic surface for different days of one WACCM3 realization. White lines indicate the poleward edge, the edge, and the equatorward edge of the polar vortex using the definition derived by *Nash et al.* [1996]. The black line indicates the area below 195 K, the approximate temperature threshold for chlorine activation.

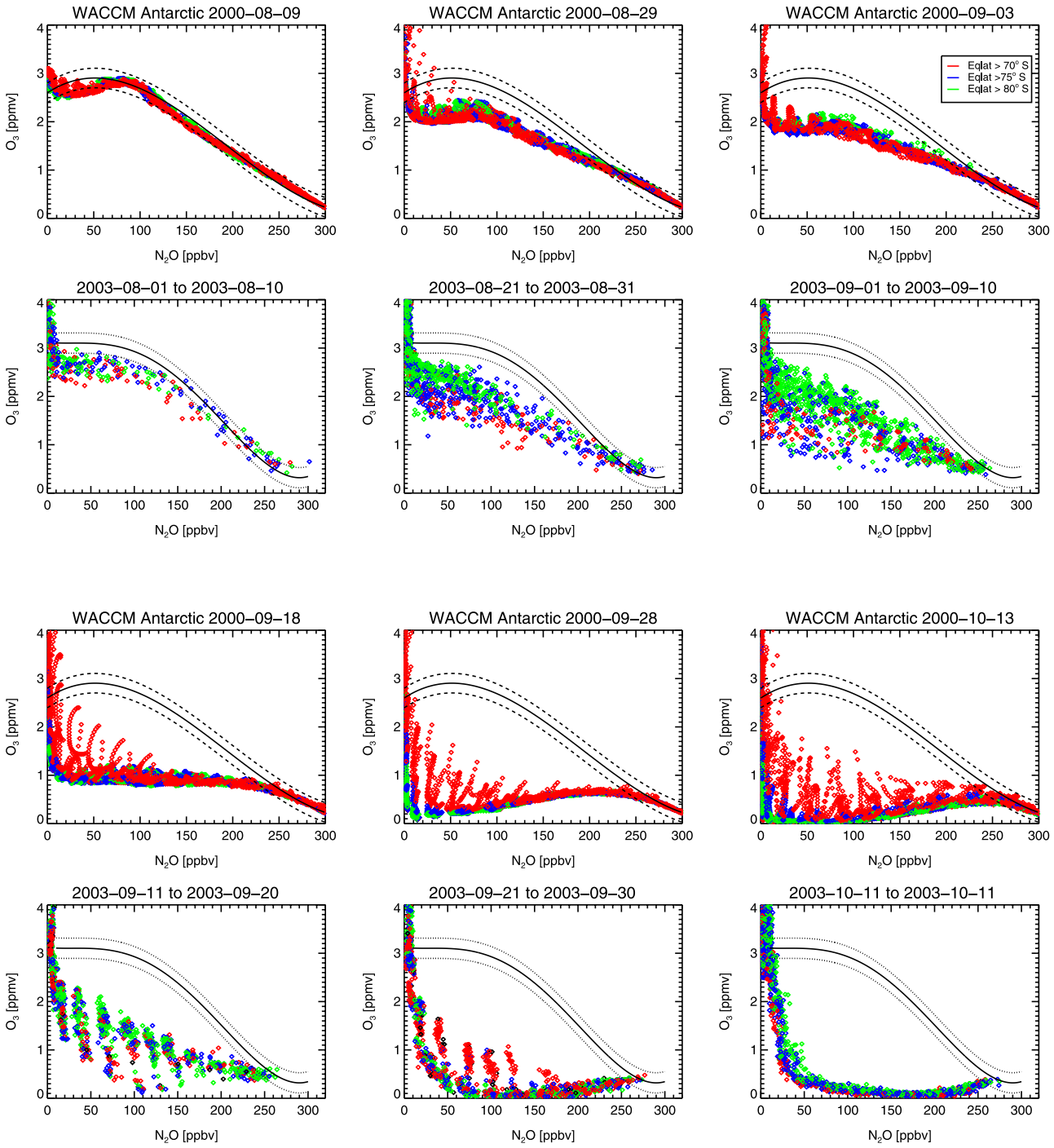

Figure 13. O_3/N_2O tracer relations for different time intervals using the third WACCM3 realization in winter 2001 (first and third row) and ILAS-II observations (second and fourth row) [*Tilmes et al.*, 2006c] for different equivalent latitudes (red: 70–75°S; blue: 75–80°S; green: 80–90°S) within the Antarctic polar vortex. The black line in each interval indicates the early winter reference function derived for the first part of July (solid line) and the area of uncertainty is surrounded by the two dashed (dotted) lines.

6.4. Accumulated Chemical Ozone Loss Between 1960 and 2003

[65] The temporal evolution of cumulative chemical ozone loss for all winters of the three model realizations between 1960 and 2003 is derived for the Arctic and Antarctica. The ensemble means for different days are shown in Figure 16. Arctic chemical ozone loss, derived using tracer-tracer correlations between mid-January and the end of March, is not reproduced using WACCM3 (see Figure 16, bottom). During March, maximum loss values do not exceed 20 DU. Observed cold Arctic winters reach more than 80 DU of column ozone loss [e.g., *Tilmes et al.*, 2006a; *Singleton et al.*, 2005]. Further, observations indicate severe ozone loss rates during January and February

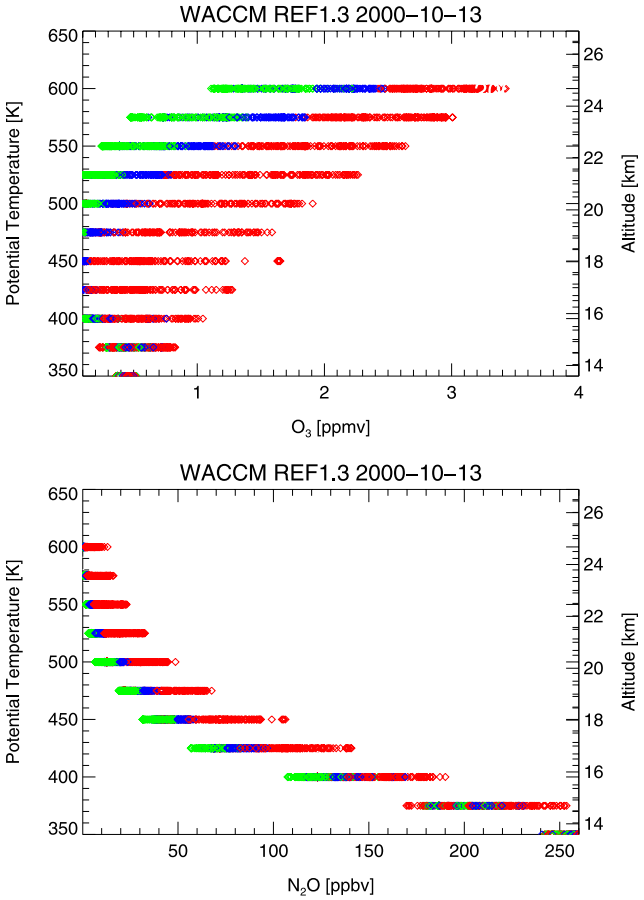

Figure 14. O_3 and N_2O profiles interpolated on different isentropic surfaces against potential temperature in 13 October 2001, using the third WACCM3 realization for different equivalent latitudes (red: 70–75°S; blue: 75–80°S; green: 80–90°S) within the Antarctic polar vortex.

substantial chlorine activation and serve ozone loss rates [e.g., *Rex et al.*, 2003]. In contrast, the meteorological conditions in WACCM3 allow chlorine activation only during February.

[66] Antarctic chemical ozone loss is derived between mid-July and the end of September. The offset of profiles in the early winter from the reference function of different equivalent latitude intervals is taken into account, as discussed above. For the Antarctic vortex core (poleward of 80°S, top), chemical ozone loss in mid-August reaches ≈20 DU and up to 80 DU in mid-September (solid and dotted lines). At the end of September, simulated chemical ozone loss within the vortex core reaches the amount of chemical ozone loss derived from HALOE observations of the 1990s. The increase of cumulative chemical ozone loss between 1960 and 1990 is simulated by WACCM3 as expected, owing to the increase of the halogen burden of the lower stratosphere [*WMO*, 2007]. The entire vortex (Figure 16, middle) chemical ozone loss is smaller than that derived from HALOE observations, as discussed above.

7. Chemical Ozone Loss and the PACl

[67] In the previous sections, meteorological diagnostics and chemical ozone loss processes were analyzed and compared between observations and simulations using WACCM3. Here, we investigate the correlation between chemical ozone loss and the potential for activation of chlorine, PACl (see section 4.1). Arctic and Antarctic chemical ozone loss from observations was derived in previous studies for winters between 1991–1992 and 2004–2005 [*Tilmes et al.*, 2006a] (see also section 3). PACl was calculated based on MetO analyses between 1991 and 2005 (as described in section 5.4). The compact relationship between cumulative chemical column ozone loss and the PACl between 1991 and 2005 derived from observations is shown as gray squares in Figure 17. Further, the proxy ozone (the column ozone in absence of chemical changes) is shown as open squares. For the Arctic, the largest observed PACl values show the strongest chemical ozone loss. For Antarctica, observed proxy ozone values are only slightly larger than chemical ozone loss values. In contrast to the Arctic, Antarctic chemical ozone loss is therefore saturated and chemical ozone loss cannot increase with increasing PACl. A detailed description of a similar relationship (assuming maximum EESC values) based on observations is given elsewhere [*Tilmes et al.*, 2006a].

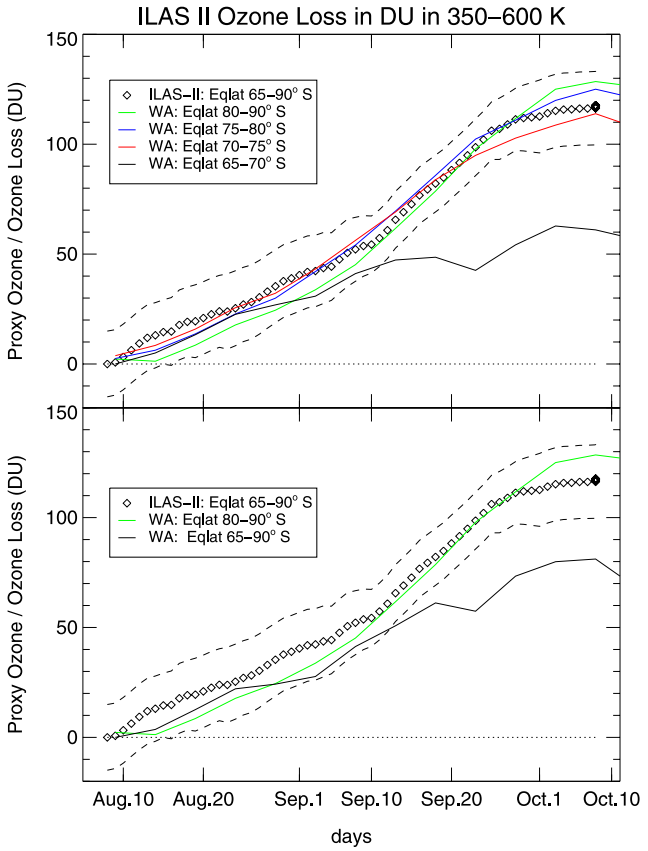

Figure 15. Temporal evolution of accumulated chemical loss in column ozone between 350 and 600 K inside the vortex core derived from ILAS-II observations, between August and October 2003 (black diamonds), smoothed over 20 d, uncertainty of ozone loss (black dashed line) [*Tilmes et al.*, 2006c]. WACCM3 accumulated chemical ozone loss for one cold Antarctic winter inside different equivalent latitude intervals (colored lines) and in the entire vortex (bottom, black line) is shown.

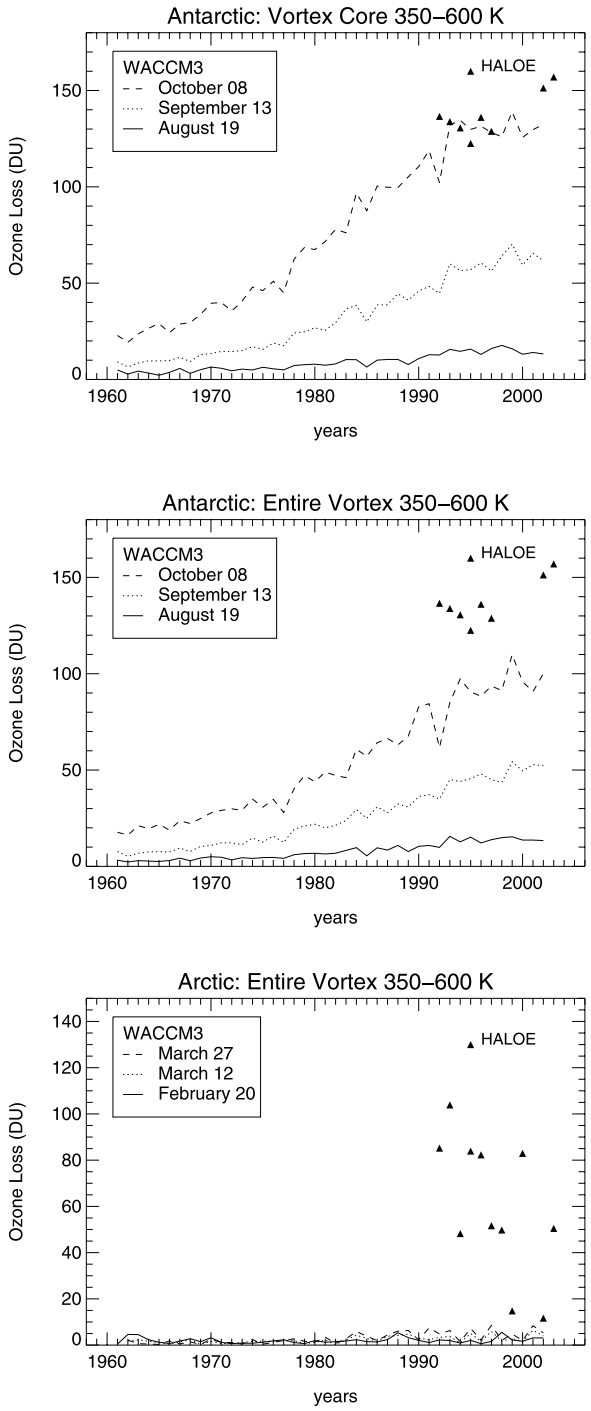

Figure 16. WACCM3 ensemble mean of accumulated chemical ozone loss between the early winter reference function and three different dates during the winter derived for the (top) Antarctic vortex core, (middle) Antarctic entire vortex, and (bottom) entire Arctic vortex, between 350 and 600 K. Different line style shows loss values around 19 August (solid), 13 September (dotted), and 8 October (dashed) for Antarctica, and loss values around 20 February (solid), 12 March (dotted), and 27 March (dashed) for the Arctic. HALOE accumulated chemical ozone at the beginning of October is shown as black triangles [*Tilmes et al.*, 2006c].

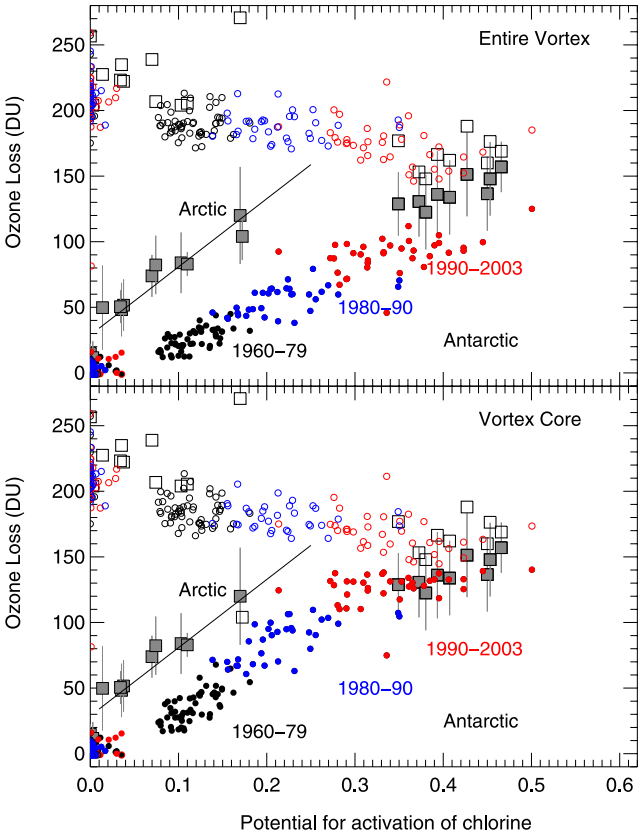

Figure 17. Relationship between the column ozone loss (DU) and potential for activation of chlorine (PACl) in the Arctic and Antarctic polar vortex for the years 1992 to 2005 derived from measurements. Monthly averaged ozone loss inside the vortex core in March in the northern hemisphere and October in the southern hemisphere between 350 and 550 K, using the tracer-tracer method and HF as the long-lived tracer (gray solid squares) and from WACCM3 simulations since 1990 (red filled circles), between 1980 and 1990 (blue filled circles) and between 1960 and 1980 (black filled circles), using N_2O as the long-lived tracer. Correspondingly, the column in proxy ozone (ozone without chemical change) is shown for each winter (open symbols). The linear relation for the Arctic from observations is shown as a black line.

[68] To compare model and observational results, the relationship between cumulative chemical column ozone loss for all three WACCM3 realizations between 1960 and 2003 is additionally plotted in Figure 17 for the entire polar vortex (top) and for the vortex core (bottom). Red symbols indicate model results for the same period as the observational results (grey and open symbols). Blue and black symbols show model results derived for the years before 1990. As for the observations, the proxy ozone is shown as open circles. For the Arctic, the WACCM3 PACl is significantly smaller than results derived from the observations. As a consequence, the cumulative chemical ozone loss in the Arctic cannot expected to reach estimated values from observations.

[69] For Antarctica, simulated PACl values are on average slightly smaller than observed between 1990 and 2003.

Chemical ozone loss values in the entire vortex do not reach observed values in the beginning of October (see Figure 16, top). WACCM3 chemical ozone loss in Antarctica is not saturated at the end of September for most of the years considered. This statement is based on the finding that ozone proxy values (column ozone without any chemical changes) are about 50 DU larger than ozone loss values. The reason for the smaller chemical ozone loss is the weaker ozone depletion in WACCM3 in the outer region of the polar vortex, as discussed above. For the vortex core, during the same period (between 1990 and 2003), chemical ozone loss is also in good agreement with observations, see Figure 17, bottom. The simulated proxy ozone is in good agreement with observations for the Arctic and Antarctica.

[70] For the years before 1990, the increase of chemical ozone loss in the Antarctic with increasing EESC, and therefore PACl values, describes a linear relationship. The slope of this relationship, derived from WACCM3 output in the vortex core region, indicates the same slope as derived for the Arctic from observations. Here, WACCM3 Antarctic chemical ozone loss values are ≈30 DU smaller than Arctic ozone loss values derived from observations.

8. Conclusions

[71] This study was performed to evaluate how well WACCM3 is able to represent chemical ozone loss in the lower polar stratosphere. The relationship between chemical ozone loss and the potential of activated chlorine (PACl) summarizes the results derived here (see Figure 17). PACl describes the meteorological conditions and the impact of changing equivalent effective stratospheric chlorine. PACl values are in approximate agreement between model and observations for Antarctica but show a large discrepancy for the Arctic. Further PACl in Antarctica is well correlated to the annual active halogen loading in the polar vortex derived from WACCM3 results.

[72] The empirical derived relationship between chemical ozone loss and PACl is not precisely reproduced in the model for both the Arctic and Antarctica. This result by itself does not identify the reasons for the shortcomings of the model. A comprehensive analysis of meteorological and chemical conditions is therefore necessary to understand the reason and sources for differences between model results and observations.

[73] A comparison was carried out between meteorological fields of three 54-year WACCM3 simulations (1950–2003) and two different meteorological analyses, MetO and ERA40. In general, seasonally averaged vortex temperatures within the polar vortex between 400 and 550 K potential temperature levels (15–25 km) agree well for Antarctica. In the Arctic the simulated temperatures are 2.5–3 K higher and have a similar annual variability. Further, the temporal evolution of temperatures between model and observations shows seasonal differences. In Antarctica, simulated temperatures are higher than observed (up to 5 degrees) at the beginning of the winter and up to 7.5 degrees lower at the end of the winter. In the Arctic the simulated temperatures are higher, especially at the beginning of the winter, which has a significant impact on the potential for activation of chlorine. Even in the coldest Arctic winter of the model simulations, WACCM3 temperatures fall below the threshold temperature for chlorine activation only between mid January and February. Further, because the simulated polar vortex is smaller compared to observations, sunlight does not reach the coldest part of the vortex area before February and catalytic cycles are not efficient in the simulation. The PACl derived using WACCM3 results only reaches values comparable to those derived for observed warm Arctic winters. Simulated chemical ozone loss does not exceed a value of 20 DU for any model realization.

[74] For Antarctica, a slightly larger WACCM3 vortex volume and slightly larger V_{ACl} than derived from the meteorological analysis result in a simulated PACl that is in good agreement with meteorological analyses. Heterogeneous processes that affect ozone loss in WACCM3 poleward of 70°S are shown to be in general agreement with observations. For one Antarctic winter, the comparison between WACCM3 model simulations and ILAS-II satellite observations shows good agreement between chemical ozone loss rates for equivalent latitudes poleward of 70°S, between August and October. On the other hand, chemical ozone loss in the outer region of the vortex, equatorward of 70°S, stops in the beginning of September, due to increasing temperatures in that region. This results in an underestimation of chemical ozone loss for the entire vortex. Further, in the early winter, simulated chemical ozone loss is delayed in the entire vortex, especially in the vortex core, owing to a weaker displacement of the vortex toward lower latitudes than observed. Insufficient illumination of the cold, activated part of the vortex in the model is responsible for the delay of the onset of chemical ozone loss.

[75] The evolution of chemical ozone loss in the Antarctic polar vortex core between 1960 and 1990 is well simulated. WACCM3 cumulative chemical ozone loss increases between 1960 and 1990 as expected, owing to the increasing of chlorine content in the stratosphere. However, ozone loss in the entire polar vortex is about one third smaller than derived from observations.

[76] Considering the product of the PV gradient and the horizontal wind velocity ($\nabla PV \cdot v$), as a measure for the transport barrier at the vortex edge, WACCM3 simulations show a much wider polar vortex edge between 65 and 80°S for Antarctica and 70 and 80°N for the Arctic than the meteorological analyses. This results in inhomogeneous tracer and temperature distributions outside the vortex core in WACCM3, with less ozone loss being diagnosed in the outer region of the vortex core, due to increasing temperatures towards the vortex edge. Further, the Arctic maximum $\nabla PV \cdot v$ is smaller in the model simulations, especially at 475 K. Mixing across the vortex edge might result in an underestimation of chemical ozone loss using tracer-tracer correlations.

[77] In summary, using WACCM3 simulations with a horizontal resolution of 4° latitude and 5° longitude does not result in a sharp edge of the polar vortex and a well mixed entire vortex as described in meteorological analysis. Future model simulations using a higher resolution are expected to improve these results. Nevertheless, it is shown that chemical processes in WACCM3 allow to simulate observed chemical ozone loss in the Antarctic polar vortex core.

[78] **Acknowledgments.** We gratefully acknowledge all members of the HALOE team at NASA Langley for providing HALOE V19 data and the science team of the ILAS-II team at NIES, Japan, led by Y. Sasano and H. Nakajima for processing ILAS-II (V1.4) data. ILAS-II data were processed at the ILAS and ILAS-II Data Handling Facility, National Institute for Environmental Studies (NIES). We gratefully acknowledge Katja Drdla for sharing her results and the formula to calculate the chlorine activation temperature. Thanks are also due to the UK Meteorological Office and the European Centre for Medium-range Weather Forecasts for providing meteorological analyses. We thank G. Bodeker for very helpful discussions on the PACl concept. S. Tilmes thanks the Deutsche Akademie der Naturforscher Leopoldina and the Bundesministerium für Bildung und Forschung for supporting this study and S. Massie and A. Gettelman for their reviews of the original manuscript.

References

Austin, J., et al. (2003), Uncertainties and assessments of chemistry-climate models of the stratosphere, *Atmos. Chem. Phys.*, *3*, 1–27.

Bodeker, G., H. Struthers, and B. Connor (2002), Dynamical containment of Antarctic ozone depletion, *Geophys. Res. Lett.*, *29*(7), 1098, doi:10.1029/2001GL014206.

Brunner, D., J. Staehelin, J. A. Maeder, I. Wohltmann, and G. Bodeker (2006), Variability and trends in total and vertically resolved stratospheric ozone based on the cato ozone data set, *Atmos. Chem. Phys.*, *6*, 4985–5008.

Burkholder, J. B., J. J. Orlando, and C. J. Howard (1990), Ultraviolet absorption cross section of Cl_2O_2 between 210 and 410 nm, *J. Phys. Chem.*, *94*, 687–695.

Carslaw, K. S., S. L. Clegg, and P. Brimblecombe (1995), A thermodynamic model of the system HCl-HNO_3-H_2SO_4-H_2O, including solubilities of HBr, from 328 K to <200 K, *J. Phys. Chem.*, *99*, 11,557–11,574.

Considine, D. B., A. R. Douglass, D. E. Kinnison, P. S. Connell, and D. A. Rotman (2000), A polar stratospheric cloud parameterization for the three dimensioal model of the global modeling initiative and its response to stratospheric aircraft emissions, *J. Geophys. Res.*, *105*, 3955–3975.

Douglas, A. R., M. R. Schoeberl, R. S. Stolarski, J. W. Waters, J. M. Russell III, A. E. Roche, and S. T. Massie (1995), Interhemispheric differences in springtime production of HCl and $ClONO_2$ in the polar vortices, *J. Geophys. Res.*, *100*, 13,967–13,978.

Drdla, K., et al. (2002), Evidence for the widespread presence of liquid-phase particles during the 1999–2000 Arctic winter, *J. Geophys. Res.*, *107*, 8318, doi:10.1029/2001JD001127. [printed *108*(D5), 2003].

Eyring, V., et al. (2005), A strategy for process-oriented validation of coupled chemistry-climate models, *Bull. Am. Meteorol. Soc.*, *86*(8), 1117–1133, doi:10.1175/BAMS-86-8-1117.

Eyring, V., et al. (2006), Assessment of temperature, trace species and ozone in chemistry-climate simulations of the recent past, *J. Geophys. Res.*, *111*, D22308, doi:10.1029/2006JD007327.

Farman, J. C., B. G. Gardiner, and J. D. Shanklin (1985), Large losses of total ozone in Antarctica reveal seasonal ClO_x/NO_x interaction, *Nature*, *315*, 207–210.

Garcia, R. R., D. R. Marsch, B. A. Boville, and F. Sassi (2007), Simulations of secular trends in the middle atmosphere, *J. Geophys. Res.*, *112*, D09301, doi:10.1029/2006JD007485.

Gillett, N. P., and D. W. J. Thompson (2002), Simulation of recent Southern Hemisphere climate change, *Science*, *302*, 273–275.

Grooß, J.-U., R. B. Pierce, P. J. Crutzen, W. L. Grose, and J. M. Russell III (1997), Re-formation of chlorine reservoirs in southern hemisphere polar spring, *J. Geophys. Res.*, *102*, 13,141–13,152.

Hanson, D. R., and K. Mauersberger (1988), Laboratory studies of the nitric acid trihydrate: Implications for the south polar stratosphere, *Geophys. Res. Lett.*, *15*(8), 855–858.

Hein, R., et al. (2001), Results of an interactively coupled atmospheric chemistry-general circulation model: Comparison with observations, *Ann. Geophys.*, *19*, 435–457.

Intergovernmental Panel on Climate Change (2001), *Climate Change 2001: The Scientific Basis*, edited by J. T. Houghton et al., 881 pp., Cambridge Univ. Press, New York.

Intergovernmental Panel on Climate Change/Technology and Economic Assessment Panel (2005), *Special Report on Safeguarding the Ozone Layer and the Global Climate System: Issues Related to Hydrofluorocarbons and Perfluorocarbons*, edited by B. Metz et al., 488 pp., Cambridge Univ. Press, New York.

Jin, J. J., et al. (2006), Severe Arctic ozone loss in the winter 2004/2005: Observations from ACE-FTS, *Geophys. Res. Lett.*, *33*, L15801, doi:10.1029/2006GL026752.

Kinnison, D. E., et al. (2007), Sensitivity of chemical tracers to meteorological parameters in the MOZART-3 chemical transport model, *J. Geophys. Res.*, *112*, D20302, doi:10.1029/2006JD007879.

Lait, L. R. (1994), An alternative form for potential vorticity, *J. Atmos. Sci.*, *51*, 1754–1759.

Langematz, U., M. Kunze, K. Krüger, K. Labitzke, and G. L. Roff (2003), Thermal and dynamical changes of the stratosphere since 1979 and their link to ozone and CO_2 changes, *J. Geophys. Res.*, *108*(D1), 4027, doi:10.1029/2002JD002069.

Lemmen, C., M. Dameris, R. Müller, and M. Riese (2006a), Chemical ozone loss in a chemistry-climate model from 1960 to 1999, *Geophys. Res. Lett.*, *33*(15), L15820, doi:10.1029/2006GL026939.

Lemmen, C., R. Müller, P. Konopka, and M. Dameris (2006b), Critique of the tracer-tracer correlation technique and its potential to analyse polar ozone loss in chemistry-climate models, *J. Geophys. Res.*, *111*, D18307, doi:10.1029/2006JD007298.

Manney, G., M. Santee, N. Livesey, L. Froidevaux, W. Read, H. Pumphrey, J. Waters, and S. Pawson (2005), EOS Microwave Limb Sounder observations of the Antarctic polar vortex breakup in 2004, *Geophys. Res. Lett.*, *32*, L12811, doi:10.1029/2005GL022823.

Manzini, E., B. Steil, C. Brühl, M. A. Giorgetta, and K. Krüger (2003), A new interactive chemistry-climate model: 2. Sensitivity of the middle atmosphere to ozone depletion and increase in greenhouse gases and implications for recent stratospheric cooling, *J. Geophys. Res.*, *108*(D14), 4429, doi:10.1029/2002JD002977.

Müller, R., S. Tilmes, P. Konopka, J.-U. Grooß, and H.-J. Jost (2005), Impact of mixing and chemical change on ozone-tracer relations in the polar vortex, *Atmos. Chem. Phys.*, *5*, 3139–3151.

Nakajima, H., et al. (2006), Characteristics and performance of the Improved Limb Atmospheric Spectrometer-II (ILAS-II) on board the ADEOS-II satellite, *J. Geophys. Res.*, *111*, D11S01, doi:10.1029/2005JD006334.

Nash, E. R., P. A. Newman, J. E. Rosenfield, and M. R. Schoeberl (1996), An objective determination of the polar vortex using Ertel's potential vorticity, *J. Geophys. Res.*, *101*, 9471–9478.

Newman, P. A., E. R. Nash, S. R. Kawa, S. A. Montzka, and S. M. Schauffler (2006), When will the Antarctic ozone hole recover?, *Geophys. Res. Lett.*, *33*, L12814, doi:10.1029/2005GL025232.

Plumb, R. A., D. W. Waugh, and M. P. Chipperfield (2000), The effect of mixing on tracer relationships in the polar vortices, *J. Geophys. Res.*, *105*, 10,047–10,062.

Proffitt, M. H., K. Aikin, J. J. Margitan, M. Loewenstein, J. R. Podolske, A. Weaver, K. R. Chan, H. Fast, and J. W. Elkins (1993), Ozone loss inside the northern polar vortex during the 1991–1992 winter, *Science*, *261*, 1150–1154.

Randel, W., et al. (2004a), The SPARC intercomparison of middle-atmosphere climatologies, *J. Clim.*, *17*, 986–1003.

Randel, W. J., F. Wu, S. J. Oltmans, K. Rosenlof, and G. E. Nodoluha (2004b), Interannual changes of stratospheric water vapor and correlations with tropical tropopause temperatures, *J. Atmos. Sci.*, *61*, 2133–2148.

Rex, M., R. J. Salawitch, M. L. Santee, J. W. Waters, K. Hoppel, and R. Bevilacqua (2003), On the unexplained stratospheric ozone losses during cold Arctic Januaries, *Geophys. Res. Lett.*, *30*(1), 1008, doi:10.1029/2002GL016008.

Rex, M., R. J. Salawitch, P. von der Gathen, N. R. Harris, M. P. Chipperfield, and B. Naujokat (2004), Arctic ozone loss and climate change, *Geophys. Res. Lett.*, *31*, L04116, doi:10.1029/2003GL018844.

Russell, J. M., L. L. Gordley, J. H. Park, S. R. Drayson, A. F. Tuck, J. E. Harries, R. J. Cicerone, P. J. Crutzen, and J. E. Frederick (1993), The Halogen Occultation Experiment, *J. Geophys. Res.*, *98*, 10,777–10,797.

Sander, S. P., et al. (2003), Chemical kinetics and photochemical data for use in atmospheric studies, *Evaluation 14, JPL Publ. 02-25*, Jet Propulsion Lab., Calif. Inst. of Technol., Pasadena.

Sassi, F., B. A. Boville, D. Kinnison, and R. Garcia (2005), The effects of interactive ozone chemistry on simulations of the middle atmosphere, *Geophys. Res. Lett.*, *32*, L07811, doi:10.1029/2004GL022131.

Shi, Q., J. T. Jayne, C. E. Kolb, and D. R. Worsnop (2001), Kinetic model for reaction of ClONO2 with H2O and HCl and HOCl with HCl in sulfuric acid solutions, *J. Geophys. Res.*, *106*, 24,259–24,274.

Shindell, D. T., and V. Grewe (2002), Separating the influence of halogen and climate changes on ozone recovery in the upper stratosphere, *J. Geophys. Res.*, *107*(D12), 4144, doi:10.1029/2001JD000420.

Simmons, A., M. Hortal, G. Kelly, A. McNally, A. Untch, and S. Uppala (2004), ECMWF analyses and forecasts of stratospheric winter polar vortex break-up: September 2002 in the southern hemisphere and related events, *J. Atmos. Sci.*, *62*(3), 668–689, doi:10.1175/JAS-3322.1.

Singleton, C. G., et al. (2005), 2002–2003 Arctic ozone loss deduced from POAM III satellite observations and the SLIMCAT chemical transport model, *Atmos. Chem. Phys.*, *5*, 597–609.

Stimpfle, R. M. (2004), First measurements of ClOOCl in the stratosphere: The coupling of ClOOCl and ClO in the Arctic polar vortex, *J. Geophys. Res.*, *109*, D03301, doi:10.1029/2003JD003811.

Swinbank, R., and A. O'Neill (1994), A stratosphere-troposphere data assimilation system, *Mon. Weather Rev.*, *122*, 686–702.

Tabazadeh, A., R. P. Turco, K. Drdla, M. Z. Jacobson, and O. B. Toon (1994), A study of type I polar stratospheric cloud formation, *Geophys. Res. Lett.*, *21*, 1619–1622.

Thomason, L., and T. Peter (Eds.) (2006), *SPARC assessment of stratospheric aerosol properties*, *Rep. 4, WCRP-124, WMO/TD-1295*, SPARC, location?.

Thomason, L. W., L. R. Poole, and T. Deshler (1997), A global climatoloy of stratospheric aerosol surface area density deduced from Stratospheric Aerosol and Gas Experiment II measurements: 1984–1994, *J. Geophys. Res.*, *102*, 8967–8976.

Thompson, D. W. J., M. P. Baldwin, and S. Solomon (2005), Stratosphere-troposphere coupling in the Southern hemisphere, *J. Atmos. Sci.*, *62*(3), 708–715.

Tilmes, S., R. Müller, J.-U. Grooß, D. S. McKenna, J. M. Russell, and Y. Sasano (2003), Calculation of chemical ozone loss in the Arctic winter 1996–1997 using ozone-tracer correlations: Comparison of Improved Limb Atmospheric Spectrometer (ILAS) and Halogen Occultation Experiment (HALOE) results, *J. Geophys. Res.*, *108*(D2), 4045, doi:10.1029/2002JD002213.

Tilmes, S., R. Müller, J.-U. Grooß, and J. M. Russell (2004), Ozone loss and chlorine activation in the Arctic winters 1991–2003 derived with the tracer-tracer correlations, *Atmos. Chem. Phys.*, *4*(8), 2181–2213.

Tilmes, S., R. Müller, A. Engel, M. Rex, and J. M. Russell III (2006a), Chemical ozone loss in the Arctic and Antarctic stratosphere between 1992 and 2005, *Geophys. Res. Lett.*, *33*, L20812, doi:10.1029/2006GL026925.

Tilmes, S., R. Müller, J.-U. Grooß, H. Nakajima, and Y. Sasano (2006b), Development of tracer relations and chemical ozone loss during the setup phase of the polar vortex, *J. Geophys. Res.*, *111*, D24S90, doi:10.1029/2005JD006726.

Tilmes, S., R. Müller, J.-U. Grooß, R. Spang, T. Sugita, H. Nakajima, and Y. Sasano (2006c), Chemical ozone loss and related processes in the Antarctic winter 2003 based on improved limb atmospheric spectrometer (ILAS)-II observations, *J. Geophys. Res.*, *111*, D11S12, doi:10.1029/2005JD006260.

Tilmes, S., R. Müller, R. Salawitch, U. Schmidt, H. Oelhaf, and J. M. Russel III (2007), Polar chemical ozone loss in the Arctic winter 1991–92, *Atmos. Chem. Phys. Discuss.*, *7*, 10,131.

Uppala, S. M., et al. (2005), The ERA-40 re-analysis, *Q. J. R. Meteorol. Soc.*, *131*, 2961–3012.

von Hobe, M., et al. (2006), Severe ozone depletion in the cold Arctic winter 2004–05, *Geophys. Res. Lett.*, *33*, L17815, doi:10.1029/2006GL026945.

World Meteorological Orgranization (2003), Scientific assessment of ozone depletion: 2002, *Rep. 47*, Geneva.

World Meteorological Orgranization (2007), Scientific assessment of ozone depletion: 2006, Global Ozone Res. and Monitor. Proj. *Rep. 50*, Geneva.

B. A. Boville, R. R. Garcia, D. E. Kinnison, D. R. Marsh, F. Sassi, and S. Tilmes, National Center for Atmospheric Research, Boulder, CO 80307, USA. (tilmes@ucar.edu)

R. Müller, Institute for Stratospheric Chemistry (ICG-1), Forschungszentrum Jülich, D-52425 Jülich, Germany.